OneDimensional Finite Elements With Arbitrary CrossSectional Displacement Fields

International Journal for Numerical Methods in Engineering

WILEY

RESEARCH ARTICLE OPEN ACCESS

One-Dimensional Finite Elements With Arbitrary Cross-Sectional Displacement Fields

E. Carrera | D. Scano | E. Zappino

MUL[2] Lab, Department of Mechanical and Aerospace Engineering, Politecnico di Torino, Torino, Italy

Correspondence: D. Scano (daniele.scano@polito.it)

Received: 19 July 2024 | **Revised:** 5 August 2025 | **Accepted:** 26 November 2025

Keywords: beam models | Carrera unified formulation | finite element method | Taylor polynomials | thin-walled structures

ABSTRACT

This paper introduces an unprecedented unified approach for developing structural theories with an arbitrary kinematic variable over the beam cross-section. Each of the three displacement variables can be analyzed using an independent expansion function. Both the order of the expansion and the number of terms in each field can be any. That is, the same order does not necessarily correspond to the same number of unknown variables. This method permits starting from a general model and write classical and known higher-order beam theories without any restrain. In this paper, the structural theories are built by using the polynomial expansion of the cross-sectional variables. The Carrera unified formulation (CUF) is employed to describe the cross-sectional kinematics. The finite element method (FEM) is employed to discretize the structure along the beam axis, utilizing Lagrange-based elements. The governing equations and related FE arrays for linear analysis are derived using the principle of virtual displacements. Both compact and thin-walled beams are examined to highlight the importance of each term of the three considered expansions. Various loading conditions, including bending, torsion, torsion-bending, and different beam slenderness ratios, are considered. The selected case studies are drawn from existing literature. The accuracy of the models presented is assessed for both displacements and stress components. The results demonstrate that the choice of the most suitable model closely depends on the specific parameters of the individual problem. That is, each structural problem has its own "best" computational models in terms of accuracy versus degree of freedom.

1 | Introduction

The section-wise deformation of beams. The development of beam theories is a classical topic in structural engineering. The preference for one-dimensional (1D) models has traditionally persisted over the introduction of more complex two-dimensional (2D) and three-dimensional (3D) analyses. Despite advancements in computational mechanics and computing power, beam models remain popular due to their relative simplicity. These models find extensive applications in engineering, ranging from aircraft wings and helicopter rotor blades in aerospace engineering to civil engineering structures composed of metallic, composites and reinforced-concrete beams.

Structures generally undergo deformation due to various parameters, such as types of loads, materials, boundary conditions, geometrical properties, and many others that can arise in specific cases [1]. Deformation pattern is a local property that depends on the specific problem under consideration. Figure 1 depicts a beam with a C cross-section loaded by forces. Three different sections are then considered. Each of them behaves in a different way from the others in the deformed state of equilibrium. That is, it is a section-wise property of the structure. The deformation of Section A is barely affected by the loads, while sections B and C experience significant deformations that are quite different from each other. That is, *it would not make sense to use the same degree of freedom for the three different sections*.

Classical and Refined beam approaches. Numerous beam models have been proposed. Notably, the classical Euler-Bernoulli [2] beam model is often used to analyze isotropic slender structures. However, it does not account for transverse shear effects. Another classical theory is the Timoshenko [3] beam model, which is capable of capturing shear effects. More details on classical beam theories are given in Section 2.1. Typically, finite element (FE) codes, especially commercial ones, employ classical 1D elements with six degrees of freedom (DOF) for each node, comprising three displacements and three rotations (3U+3R), as illustrated in Figure 2. For further details, interested readers can refer to the book by Bathe [4].

Classical beam elements are limited in accurately describing local effects and nonlinear deformations. A more effective solution is achieved by employing 3D elements, even though this comes with increased computational costs (see Argyris [5]). In these 3D elements, only three displacements (3U) are used for each FE node, as illustrated in Figure 3a for a C-section beam. A classical brick eight-node element is shown. Furthermore, plate/shell (2D) elements are commonly used to study thin-walled structures, as shown in Figure 3b, where a classical four-node element is shown. Both five- and six-DOF elements for each node have been developed in the literature. See Bathe and Ho [6] for more information. It is also possible to simultaneously adopt 3D and 2D FE elements, see Surana [7, 8]. Also, 1D and 3D FE elements have

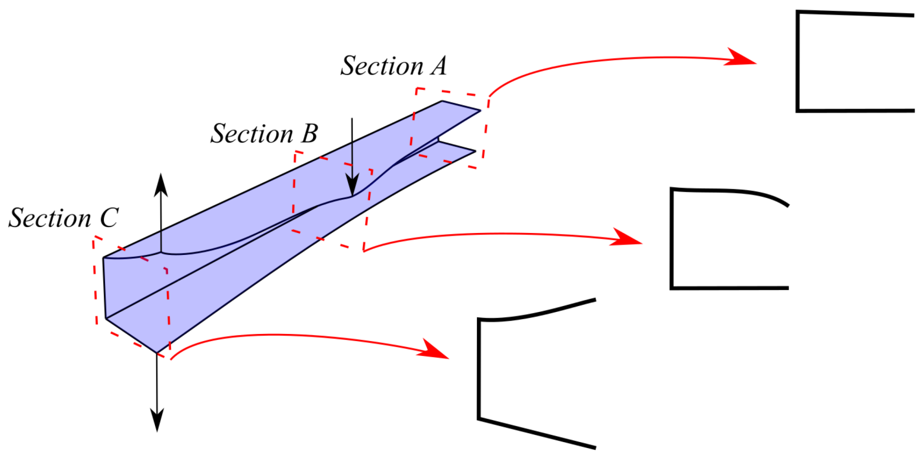

FIGURE 1 | Localized deformations on different sections of a beam structure.

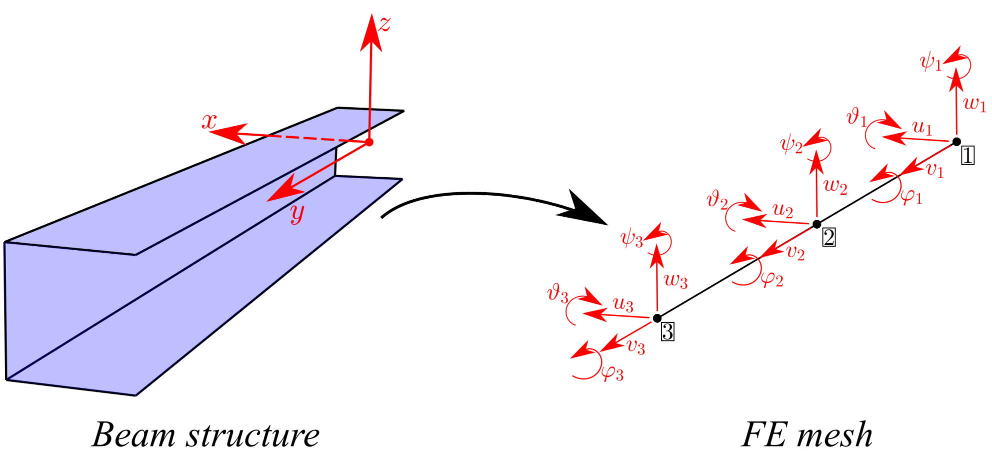

FIGURE 2 | Classical one-dimensional finite elements.

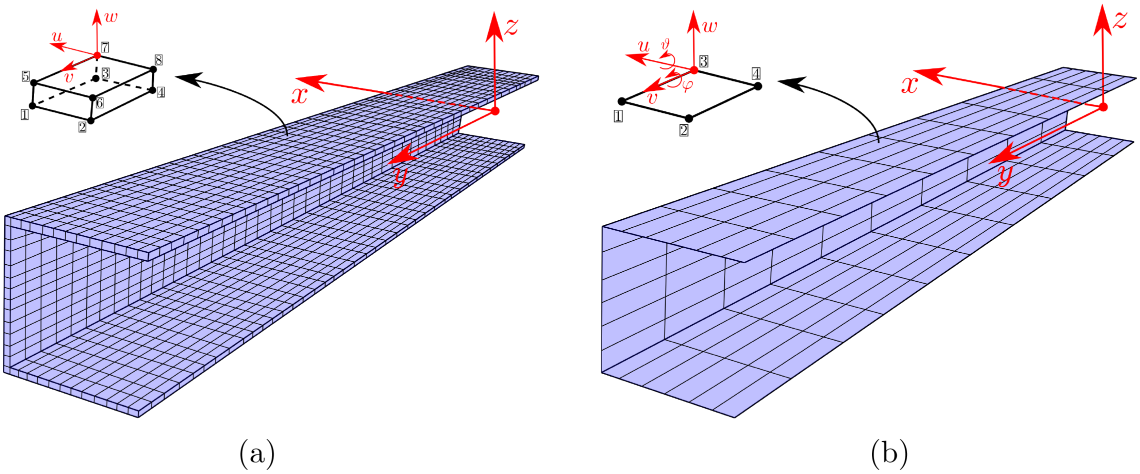

FIGURE 3 | Use of three-dimensional (a) and plate/shell (b) finite elements to discretize beam-like structures. (a) Three-dimensional mesh, (b) Bi-dimensional mesh.

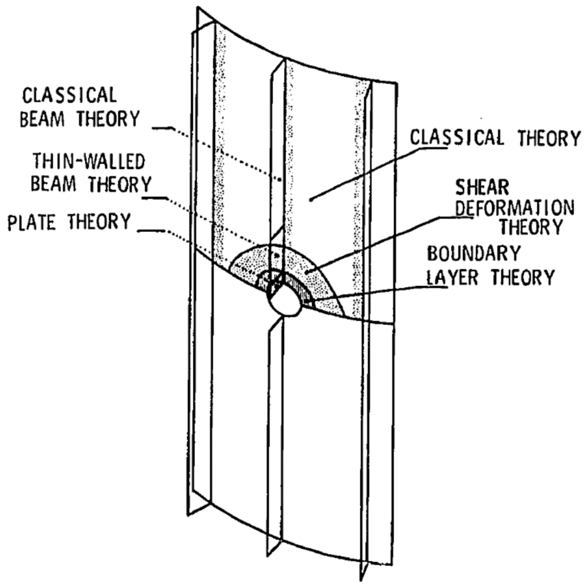

FIGURE 4 | Use of a global-local method to discretize a structure, reported from Noor [10].

been connected in the same model, as investigated in Gmür and Kauten [9]. In this way, the computational costs can be diminished and the efficiency increases. To facilitate this integration, global/local methods have been implemented, as reviewed by Noor [10]. Figure 4 illustrates a structure discretized with several models.

Various refined beam models have been proposed to overcome the limitations of classical beam theories. First, the so-called axiomatic theories are briefly reviewed, where scientists made 'a priori' or 'intuitive' assumptions for the deformed states of the loaded structures. For instance, see Novozhilov's influential book [11]. Comprehensive reviews of advanced beam models can be found in the works of Kapania and Raciti [12, 13] and Carrera et al. [14]. Additional insights into higher-order beam theories were provided by Washizu [15]. The most general refined theory can be written as the following polynomial expansion:

$$
\begin{aligned}
u_x &= u_{x_1} + x u_{x_2} + z u_{x_3} + x^2 u_{x_4} + xz u_{x_5} + z^2 u_{x_6} + \cdots + x^a z^b u_{x_N} \\
u_y &= u_{y_1} + x u_{y_2} + z u_{y_3} + x^2 u_{y_4} + xz u_{y_5} + z^2 u_{y_6} + \cdots + x^a z^b u_{y_N} \\
u_z &= u_{z_1} + x u_{z_2} + z u_{z_3} + x^2 u_{z_4} + xz u_{z_5} + z^2 u_{z_6} + \cdots + x^a z^b u_{z_N}
\end{aligned} \tag{1}
$$

Furthermore, Vlasov [16] introduced the use of warping functions to account for cross-section deformation, enabling the analysis of thin-walled structures. This method has been employed by Friberg [17], Ambrosini et al. [18], and Mechab et al. [19]. Another approach, known as Generalized Beam Theory (GBT), was proposed by Schardt [20]. GBT improves classical theories by using piece-wise beam descriptions of thin-wall sections, which permit capturing complex phenomena like warping and distortional effects. Ganapathi et al. [21] developed a three-node beam FE that includes transverse shear and warping torsion. This approach addresses shear deformation using a higher-order cosine function. Levinson [22] proposed a new beam theory that incorporates cross-section warping while respecting shear-free conditions on the lateral surfaces. Heyliger and Reddy [23] utilized this theory to create a locking-free beam element. Kant and Manjunath [24] introduced higher-order displacement models using the C^0 FE method to analyze laminated composite beams. They varied the displacement component along the axis direction from first to fourth order while keeping the displacement component in the thickness direction constant, similar to classical models. Further refinements were proposed by the same authors in [25] and [26], where they assumed higher-order terms for the transverse displacement.

Mallikarjuna and Kant [27] used five different plate higher-order shear deformable theories to study free vibrations and transient dynamics for laminated composites and sandwiches. Kapania and Goyal [28] proposed a two-node beam element to study the dynamic response of unsymmetrically laminated beams with uncertainties in the ply orientations. Eight DOF are considered for each FE node. On the other hand, Kapania and Raciti [29] adopted 10 DOF for each node to focus on nonlinear vibrations of laminated structures. Considering the geometrical non-linearities, Machado [30] studied the post-buckling of thin-walled beams. Each displacement variable is studied by different expansion functions, including trigonometric terms. Mohri et al. [31] proposed a FE beam with seven DOF for each node, which accounted for large torsion and warping effects. Xie et al. [32] implemented a general higher-order shear deformation zig-zag plate theory in aerothermoelastic. It is capable to reduce to several literature plate models. However, the transverse displacement is not able to account for higher-order effect. Finally, papers regarding the constitutive non-linearities are taken into account. Amambres et al. [33] studied elastic-plastic thin-walled beams by using a GBT-based model. Simo et al. [34] proposed an advanced kinematic model starting from the solution of Saint Venant's problem. In this reference, the elasto-viscoplastic response of beams is studied considering the shear effects. Salomon et al. [35] focused on the fracture analysis of beams with the use of Levinson [22] higher-order theory.

The Carrera Unified Formulation vs axiomatic and asymptotic approaches. Finally, the Carrera unified formulation (CUF) was proposed by Carrera [36] for plate and shells. By employing this approach, many problems have been studied, such as the normal stress effects [37] or large-deflection and post-buckling analyses [38]. The CUF was extended for the beam formulation by Carrera and Giunta [39]. In the CUF framework, cross-section kinematics can be approximated using various types of functions. Carrera et al. [40] utilized Taylor-like expansions up to the fourth order to analyze compact and thin-walled airfoil sections. Additionally, Carrera et al. [41] demonstrated the enhanced capabilities of higher-order theories in the study of shell-like structures. Carrera and Petrolo [42] introduced three-, four-, and nine-node Lagrange-like expansions to investigate composite beams.

Some of the most remarkable asymptotic contributions to beam theories deserve attention as well. The asymptotic method uses an expansion of an important parameter of the structure (e.g., the length-to-thickness ratio of the beam) to develop refined 1D theories. This methodology uses variationally consistent and geometrically exact governing equations leading to asymptotically exact results, while using a relatively low number of DOF. In [43], Volovoi et al. investigated open cross-section and thin-walled structures by applying the variational-asymptotic method (VAM) to analyze open cross-section, thin-walled anisotropic beams. 3D models were used as a comparison to assess the results. Volovoi and Hodges [44] introduced an extension to beams with generally contoured cross-sections. On the other hand, Popescu and Hodges [45] employed the VAM to develop a refined beam theory capable of considering shear deformations. This theory enables the analysis of structural problems involving arbitrary general cross-sections. Berdichevsky [46] introduced the VAM, which builds an asymptotic expansion of the solution using a characteristic cross-section parameter. This method was further adopted by Giavotto et al. [47]. Additionally, Živković et al. [48] introduced a general beam formulation that incorporates cross-sectional deformation. Yoon and Lee [49] introduced a similar approach capable of studying both in-plane and out-of-plane warping. Yu et al. [50] introduced a method to address anisotropic beams with general cross-sections in a FE framework, considering initially curved and twisted beams. The validation of the Variational Asymptotic Beam Sectional Analysis (VABS) computer program was reported by Yu et al. [51].

Aim of the present paper. In the previous literature works, scholars proposed ad hoc theories, which were able to accurately predict specific structural behaviors. For instance, thin-walled beams require very advanced models. To this end, for each problem, the scholars have to redefine a new theory and recalculate the governing equations. Some frameworks,

TABLE 1 | Complete fourth-order Taylor theory, Number of Terms = 45.

Variable	Constant	Linear		Parabolic			Cubic				Quartic				
	1	x	z	x^2	xz	z^2	x^3	x^2z	xz^2	z^3	x^4	x^3z	x^2z^2	xz^3	z^4
u_x	●	●	●	●	●	●	●	●	●	●	●	●	●	●	●
u_y	●	●	●	●	●	●	●	●	●	●	●	●	●	●	●
u_z	●	●	●	●	●	●	●	●	●	●	●	●	●	●	●

TABLE 2 | Example of a reduced fourth-order Taylor theory, Number of Terms = 11.

Variable	Constant	Linear		Parabolic			Cubic				Quartic				
	1	x	z	x^2	xz	z^2	x^3	x^2z	xz^2	z^3	x^4	x^3z	x^2z^2	xz^3	z^4
u_x	∘	∘	∘	∘	●	∘	●	∘	∘	∘	∘	∘	∘	●	∘
u_y	∘	∘	●	●	∘	∘	∘	∘	∘	●	∘	∘	∘	∘	∘
u_z	●	∘	∘	∘	∘	●	∘	∘	∘	∘	●	∘	●	∘	●

notably the GBT and the CUF, tried to create a unique formulation to study the structures, and so have the possibilities to choose several models without changes to the general mathematical assumptions. However, even though the results are very interesting, they are not able to evaluate the impact of each term within the expansion. Thus, the aim of this work is to propose a consistent formulation, where the user may use the desired theory with the desired accuracy. Such an analysis appears to be the only way to fit with the 'section-wise deformation' described at the beginning of this introductory part. In structural problem-solving, computational cost stands as a pivotal aspect. Therefore, obtaining dependable results at minimum expense holds considerable interest. In this paper, thus, it is possible to use both complete Taylor expansions and the so-called *reduced* models.

The generation of reduced theories can be visually depicted. Table 1 showcases a complete fourth-order Taylor theory, with bullets denoting the included terms across the three displacement variables. This uniform theory employs 45 terms. However, the impact of individual terms can be studied. By selectively considering or disregarding terms, researchers can build reduced models. Table 2 illustrates a fourth-order model where only 11 terms are included. The circles indicate the disregarded terms. To make the concept more understandable, the explicit expansion equations are presented in the Appendix A. Considering the example given in Figure 1, Figure 5 illustrates the three sections of the beam. Each section could be studied by an *ad hoc* model, to better represent the section-wise behavior of the deformation. As it is obvious, for the analysis of section C, the most refined model with 15 terms could be efficiently employed.

In recent years, the asymptotic-axiomatic method (AAM) has been proposed, see [52] for further details. The name stems from employing a fixed framework, allowing for the investigation of the role of each term while varying multiple parameters such as loading conditions and length-to-thickness ratios.

Using this method, a two-dimensional plot can be built, as depicted in Figure 6a. The error relative to the reference solution is displayed on the horizontal axis, while the number of considered terms is indicated on the y-axis. Four models are explicitly written for the sake of clarity. This method allows to build the best theory diagram (BTD), which is the curve that identifies all the models with the least error for a given number of terms, see Figure 6b. Essentially, it represents a Pareto Front. In this example, a complete fourth-order model (TE4) serves as the reference solution. Furthermore, it is possible to represent the uniform theories, where all three displacement variables adopt the same complete expansion. With the same method, one can estimate the errors of the literature models: first-order torsion model [15], 6-DOF used in the classical FE codes, TBM [3], and HOSTB8 [26], that consists of eight terms. Notably, this graph possesses two key properties: (a) it is problem-dependent; (b) it changes according to the desired output. Finally, it is worth noting how the model 'd' (11) of the Figure 6a considers some four-order terms, while the complete expansion TE4 must include all 45 terms.

In existing literature, a unified method for the automatic generation of reduced beam models, such as those illustrated in Table 2, is yet to be proposed. This is critical for obtaining the most efficient computational model, minimizing the number of DOF while maintaining a fixed level of accuracy. In recent years, numerous studies within the context of the

Section A

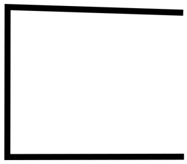

Variable	constant	linear		parabolic		
	1	x	z	x^2	xz	z^2
u_x	●	○	○	○	○	○
u_y	●	●	●	○	○	○
u_z	●	○	○	○	○	○

Section B

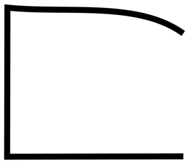

Variable	constant	linear		parabolic		
	1	x	z	x^2	xz	z^2
u_x	●	●	●	●	○	○
u_y	●	●	●	○	○	○
u_z	●	●	●	○	○	○

Section C

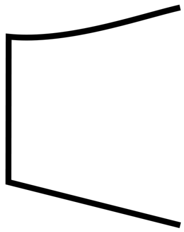

Variable	constant	linear		parabolic		
	1	x	z	x^2	xz	z^2
u_x	●	●	●	●	●	●
u_y	●	●	●	○	○	○
u_z	●	●	●	●	●	●

FIGURE 5 | Use of different reduced models for the study of the three sections of Figure 1.

CUF simulated the creation of reduced models through penalization techniques. In this way, the meaning of terms in displacement variables is investigated. Carrera and Petrolo [52] examined the efficacy of terms in Taylor-based expansions within the beam formulation for the displacement and stresses. As said before, terms were selectively eliminated using a penalization technique. However, the stiffness matrix always had the dimension of the most accurate theory. Thence, the effective DOF is always the same. For instance, referring again to Table 1, all the analyses, from a computational perspective, actually have 45 terms for each FE node. This same approach has been adopted for plate and shell formulations in various works. Notably, in these cases, one-dimensional expansions along the thickness direction were employed. For more details, refer to [53] and [54].

In contrast, Demasi [55] introduced the Generalized Unified Formulation (GUF) for analyzing *plate* structures for closed-form solution. Then, the GUF was extended by the same author [56] to a two-dimensional FE framework. In this approach, the 3×3 fundamental nucleus (FN) of the stiffness matrix is replaced by a scalar FN. This reformulation allows for the reordering of the global stiffness matrix, facilitating the independent definition of displacements. This formulation has been used in a geometrical nonlinear framework in Santarpia and Demasi [57]. In the present paper, however, the beam formulation is illustrated, which can easily handle structures with complicated cross-sections. Furthermore, the polynomial terms of the complete Taylor expansions may be selectively disregarded.

Proposal for determining the best computational model. This paper serves as the initial step toward developing a method for systematically determining the most suitable model for beam formulation. Companion papers outlining further steps will be presented in the future. These steps can be summarized as follows:

a. The present paper establishes the theoretical foundations for creating reduced models. Currently, identical models are utilized across all the beams length.

b. A method to analyze the beam section-wise is employed, wherein every section is approximated by a different structural theory. For instance, the node-dependent kinematics (NDK) approach can be implemented using CUF capabilities [1]. As the name suggests, NDK allows for choosing the expansion theory for each FE node. Thus, the reduced models and NDK will be used in synergy.

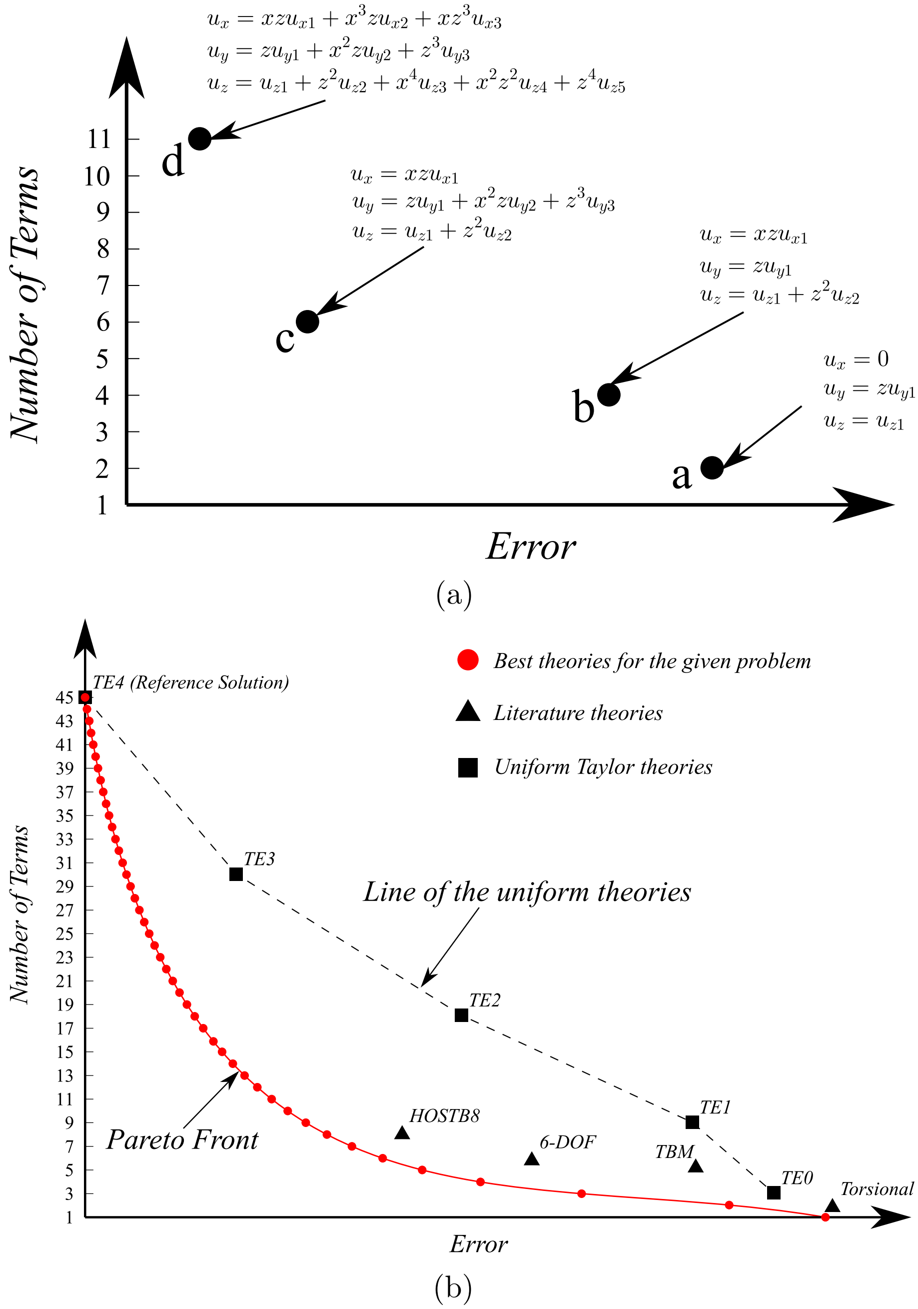

FIGURE 6 | Representation of in a 2D plot Error-Number of Terms (a) and example of a Best Theory Diagram (b). (a) Four beam theories, (b) Best Theory Diagram.

c. A method to analyze and classify the proposed theories can be accomplished through the AAM. The first step is to represent the AAM only for models equal along the beam. Then, the AAM is used in conjunction with the NDK method. Some attempts have been made in the CUF literature [58]. The objective is to compare all the combinations and insert them into a diagram.

d. To systematically analyze this information and reduce analysis time, innovative techniques such as data mining and machine learning can be employed. As the number of theory combinations can be substantial, dealing with complex structures might become unfeasible. For instance, genetic algorithms and neural networks have been utilized in CUF literature [53, 58] for determining the best theories.

e. The ultimate goal would be to create a database from which to train a neural network. This tool could then indicate the best model for a given accuracy, taking into account boundary conditions, loadings, materials, and other known characteristics.

Contents of this work. All these steps will be proposed and integrated in a single framework by employing the possibilities of CUF in this and subsequent works.

This work proposes Equation (1), based on the framework of CUF. The applicability of this equation can be tailored to specific theories, as exemplified in Table 2. To make this possible, the authors started from the concept of the CUF, where it is possible to create refined models from the same mathematical framework, without rewriting the governing equations every time the displacement field changes. However, in the 'classical' CUF, the displacement variables are studied by the same expansion function. This fact is a limitation to the possibility of creating 'ad hoc' theories and choose the desired degree of accuracy and limit the computational costs. To this end, the unified formulation has been redefined to ease the creation of specialized beam theories within the FE method. A scalar FN is employed as the basis for constructing the global stiffness matrix, avoiding the exclusion of terms through penalization techniques, as implemented in [52]. This approach enables the derivation of a stiffness matrix with consistent dimensions, that is, the effective dimension of the stiffness matrix (and of the unknown and load vectors) is dependent on the kinematic model. Finally, the primary focus of this introductory paper is the analysis of isotropic structures, spanning from compact to thin-walled beams.

This paper is structured as follows: (a) Section 2 provides an overview of several classical beam theories from the literature. Also, Taylor-based expansions are illustrated. In particular, the concept of *reduced* theories is explained. (b) Section 3 illustrates the principles of the Unified formulation approximation and the union with the finite element method (FEM). (c) In Section 4, the governing equations are derived by adopting the principle of virtual displacements. (d) Section 5 shows how to assemble the stiffness matrix and the load vector with the Unified formulation through a practical example. (e) In Section 6, results for the displacements and stresses are displayed. (f) Finally, the major conclusions are summarized in Section 7.

2 | Review of the Beam Theories

Consider the isotropic beam depicted in Figure 7. A Cartesian reference system is adopted. The cross-section, A, lies in the x-z plane. On the other hand, the beam axis, denoted as L, is aligned with the y direction. The three-dimensional displacement field is described by the following vector:

$$\mathbf{u}(x, y, z) = \left\{ u_x(x, y, z),\ u_y(x, y, z),\ u_z(x, y, z) \right\}^T \tag{2}$$

As anticipated in the Introduction section, scholars have proposed several models to describe the displacement variables. It is worth noting that u_x, u_y, and u_z can be explicitly written with different theories, similar to the classical models.

This section explicitly presents and describes several classical and refined theories mentioned in the Introduction. Additionally, these models are presented in accordance with the reference system depicted in Figure 7.

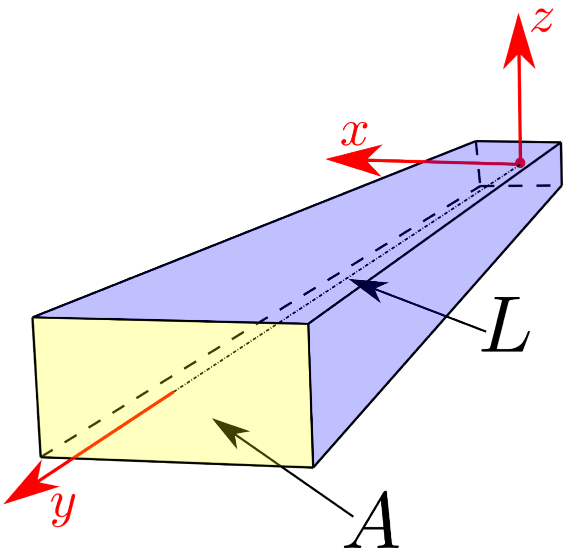

FIGURE 7 | Reference system for a generic beam-like structure.

2.1 | Classical Beam Theories

One of the most known displacement-based theory is the Euler-Bernoulli [2] Beam Model (EBBM) expressed as follows:

$$
\begin{aligned}
u_x(x, y, z) &= u_{x_1}(y) \\
u_y(x, y, z) &= u_{y_1}(y) + \frac{\partial u_{x_1}(y)}{\partial y} x - \frac{\partial u_{z_1}(y)}{\partial y} z \\
u_z(x, y, z) &= u_{z_1}(y)
\end{aligned} \tag{3}
$$

On the other hand, the displacement field of the Timoshenko [3] Beam Model (TBM) reads:

$$
\begin{aligned}
u_x(x, y, z) &= u_{x_1}(y) \\
u_y(x, y, z) &= u_{y_1}(y) - \phi_z(y)x + \phi_x(y)z \\
u_z(x, y, z) &= u_{z_1}(y)
\end{aligned} \tag{4}
$$

where u_{x_1}, u_{y_1}, and u_{z_1} represent the displacement of the beam axis, whereas ϕ_z and ϕ_x denote rotations around the z and x axes, respectively. Additionally, $-\frac{\partial u_{x_1}(y)}{\partial y}$ and $\frac{\partial u_{z_1}(y)}{\partial y}$ correspond to rotations around the z and x axes when the cross-section remains planar and orthogonal to the line axis.

In addition to the limitations outlined in the Introduction, other drawbacks are present in EBBM and TBM theories. For instance, they are not capable to analyze the structures when torsional moments are applied. The simplest torsion theory (see Washizu [15]) may be expressed as follows:

$$
\begin{aligned}
u_x(x, y, z) &= z\theta \\
u_y(x, y, z) &= 0 \\
u_z(x, y, z) &= -x\theta
\end{aligned} \tag{5}
$$

2.2 | Some Higher-Order Theories

When focusing on purely bending problems, it is possible to use simplified models where the influence of the x direction is entirely disregarded. Consequently, the variable u_x is omitted, and terms with x^a are not considered. Manjunatha and Kant [26] introduced a range of HOTs in this context. For instance, the following set can be adopted in the symmetric sections:

$$
\begin{aligned}
u_y &= z\theta_y(y) + z^3\theta_y^*(y) \\
u_z &= u_{z_0}(y)
\end{aligned} \tag{6}
$$

Furthermore, a second-order expansion for the variable u_z can be taken in account as follows:

$$
\begin{aligned}
u_y &= z\theta_y(y) + z^3\theta_y^*(y) \\
u_z &= u_{z_0}(y) + z^2 u_{z_0}^*(y)
\end{aligned} \tag{7}
$$

The previous formulas serve as excellent examples of how scholars can customize beam models to effectively analyze bending problems with a general reduction in DOF. These concepts will be further elucidated in the following Section 2.3, where Taylor-based models are presented.

2.2.1 | Example for Shear Stresses of a Bending Beam

An example is given to understand the possibilities of ad hoc reduced modules. For instance, it is possible to reproduce a model similar to those proposed by Manjunatha and Kant [26]. The displacement field can be written as follows:

$$
\begin{aligned}
u_y &= u_{y_1} + z u_{y_2} + z^2 u_{y_3} + z^3 u_{y_4} \\
u_z &= u_{z_1} + z u_{z_2} + z^2 u_{z_3}
\end{aligned} \tag{8}
$$

where u_y adopts a cubic expansion, whereas u_z uses a second-order polynomial.

The shear stresses σ_{yz} for an isotropic beam holds:

$$\sigma_{yz} = G\epsilon_{yz} \tag{9}$$

where G denotes the shear modulus. Therefore, the only quantity to be evaluated is the shear strain, ϵ_{yz}, as follows:

$$\epsilon_{yz} = \frac{\partial u_y}{\partial z} + \frac{\partial u_z}{\partial y} = u_{y_2} + 2zu_{y_3} + 3z^2 u_{y_4} + u_{z_1,y} + zu_{z_2,y} + z^2 u_{z_3,y} \tag{10}$$

This approach enables the determination of the actual distribution of shear stresses, which, for an isotropic compact section, is parabolic.

2.3 | Taylor-Based Higher-Order Theories

Taylor polynomials, specifically 2D polynomials of the form $x^a z^b$, are employed to formulate general Higher-Order Theories (HOTs) for describing the behavior of beam cross-sections. These polynomials use positive integers for both a and b. Within the context of the CUF, Carrera and Giunta [39] initially investigated beams from the first to the fourth orders to account for higher-order effects. When adopting first-order models, Poisson locking is mitigated through the appropriate reduction of material stiffness coefficients.

2.3.1 | Uniform Theories

In the literature concerning the CUF for the beam formulations, a uniform expansion is assumed for all three displacement variables. These models are referred to as *uniform theories*. For instance, a second-order theory can be expressed as follows:

$$\begin{aligned} u_x &= u_{x_1} + xu_{x_2} + zu_{x_3} + x^2 u_{x_4} + xzu_{x_5} + z^2 u_{x_6} \\ u_y &= u_{y_1} + xu_{y_2} + zu_{y_3} + x^2 u_{y_4} + xzu_{y_5} + z^2 u_{y_6} \\ u_z &= u_{z_1} + xu_{z_2} + zu_{z_3} + x^2 u_{z_4} + xzu_{z_5} + z^2 u_{z_6} \end{aligned} \tag{11}$$

2.3.2 | Different Theories

Previous uniform theories presented identical expansions for all three variables. However, this paper also presents results where u_x, u_y, and u_z are approximated by different polynomial orders. For example, the following structural theory is described by a first-order expansion for u_x and u_z, while a second-order expansion is adopted for u_y:

$$\begin{aligned} u_x &= u_{x_1} + xu_{x_2} + zu_{x_3} \\ u_y &= u_{y_1} + xu_{y_2} + zu_{y_3} + x^2 u_{y_4} + xzu_{y_5} + z^2 u_{y_6} \\ u_z &= u_{z_1} + xu_{z_2} + zu_{z_3} \end{aligned} \tag{12}$$

Thus, this theory is composed of 12 terms, in contrast to the uniform second-order theory Equation (11), which contains 18 expansion functions.

2.3.3 | Reduced Theories

In the uniform and different theories, complete Taylor expansions are illustrated. This means that all the terms are present in the single displacement variable. However, it is apparent from physical considerations that some terms can be disregarded. In this way, the so-called *reduced theories* can be built, as in the following:

$$\begin{aligned} u_x &= u_{x_1} + zu_{x_2} \\ u_y &= u_{y_1} + xu_{y_2} + xzu_{y_3} + z^2 u_{y_4} \\ u_z &= u_{z_1} \end{aligned} \tag{13}$$

Please take note of the distinctions in the u_y variable between Equation (11) (or (12)) and Equation (13). In the former, all six terms are retained, while the reduced model only considers four terms. Consequently, the subscripts are adjusted. In general, taking also into account the u_x and u_z variables, seven terms are retained, resulting in a significant reduction in DOF compared to the uniform theory.

In the CUF literature, the removal of a term is achieved through a penalization technique, which starts from a complete uniform theory. Consequently, the effective number of terms remains constant. For a more detailed explanation, please refer to [59].

3 | Unified Formulation for Beam and Generalization to the Higher-Order Theories

In the previous sections, several models from the literature have been shown. In addition to this, it is possible to create new *ad hoc* models. The CUF has the special capability to describe all these models in a compact manner, starting from the same mathematical framework. In the CUF, a 3D problem is condensed into a 1D framework. In this context, a general variable (such as displacement, stress, or strain component) denoted as f is expressed in terms of one or more additional variables f_τ (where $\tau = 1, \dots, M$). These additional variables are defined at specific locations on the beam section, typically corresponding to the beam's axis. This expansion is constructed by introducing base functions $F_\tau(x,z)$, which are defined over the beam section, and can be expressed using the following formula:

$$f(x,y,z) = \sum_{\tau=1}^{M} F_\tau(x,z) f_\tau(y) = F_\tau(x,z) f_\tau(y), \qquad \tau = 1, 2, \dots, M \tag{14}$$

Hereinafter, Einstein's summation is employed whenever two dummy indices are present.

The 3D displacement field is represented as a general expansion of the primary mechanical variables, achieved by employing arbitrary functions defined over the domain for each displacement variable:

$$\begin{aligned} u_x &= F_{u_x\tau}(x,z) u_{x_\tau}(y) \ \text{ with } \ \tau = 1, \dots, M_{u_x} \\ u_y &= F_{u_y\tau}(x,z) u_{y_\tau}(y) \ \text{ with } \ \tau = 1, \dots, M_{u_y} \\ u_z &= F_{u_z\tau}(x,z) u_{z_\tau}(y) \ \text{ with } \ \tau = 1, \dots, M_{u_z}. \end{aligned} \tag{15}$$

$F_{u_x\tau}$, $F_{u_y\tau}$, and $F_{u_z\tau}$ represent the expansion functions for the generalized displacements u_{x_τ}, u_{y_τ}, and u_{z_τ}, respectively. In previous CUF-based works [39, 41], the expansions were simply denoted as F_τ since all three displacement variables utilized the same model. The symbol τ represents summation, and M_{u_x}, M_{u_y}, and M_{u_z} indicate the number of expansions for each displacement variable. It is important to note that the value of τ changes depending on the specific component being considered.

Since the Principle of the Virtual Displacement (PVD) will be adopted to derive the governing equations, it is essential to calculate the virtual displacements as follows:

$$\begin{aligned} \delta u_x &= F_{u_x s}(x,z) \delta u_{x_s}(y) \ \text{ with } \ s = 1, \dots, M_{u_x} \\ \delta u_y &= F_{u_y s}(x,z) \delta u_{y_s}(y) \ \text{ with } \ s = 1, \dots, M_{u_y} \\ \delta u_z &= F_{u_z s}(x,z) \delta u_{z_s}(y) \ \text{ with } \ s = 1, \dots, M_{u_z}. \end{aligned} \tag{16}$$

where $F_{u_x s}$, $F_{u_y s}$, and $F_{u_z s}$ are the expansion functions in the virtual system. As can be noted, the subscript τ is replaced by s.

The CUF approximation and the FEM can be effectively combined to obtain numerical results. FEM is employed to discretize the displacements along the beam axis. Within this framework, the displacements can be expressed as shown below:

$$u_x = N_i(y) F_{u_x \tau}(x,z) q_{x_{\tau i}} \quad \text{with} \quad \tau = 1, \dots, M_{u_x} \quad \text{and} \quad i = 1, \dots, N_n$$

$$u_y = N_i(y) F_{u_y \tau}(x,z) q_{y_{\tau i}} \quad \text{with} \quad \tau = 1, \dots, M_{u_y} \quad \text{and} \quad i = 1, \dots, N_n$$

$$u_z = N_i(y) F_{u_z \tau}(x,z) q_{z_{\tau i}} \quad \text{with} \quad \tau = 1, \dots, M_{u_z} \quad \text{and} \quad i = 1, \dots, N_n. \tag{17}$$

and their virtual variations read:

$$\delta u_x = N_j(y) F_{u_x s}(x,z) \delta q_{x_{sj}} \quad \text{with} \quad s = 1, \dots, M_{u_x} \quad \text{and} \quad j = 1, \dots, N_n$$

$$\delta u_y = N_j(y) F_{u_y s}(x,z) \delta q_{y_{sj}} \quad \text{with} \quad s = 1, \dots, M_{u_y} \quad \text{and} \quad j = 1, \dots, N_n$$

$$\delta u_z = N_j(y) F_{u_z s}(x,z) \delta q_{z_{sj}} \quad \text{with} \quad s = 1, \dots, M_{u_z} \quad \text{and} \quad j = 1, \dots, N_n. \tag{18}$$

where N_i and N_j stand for the shape functions. The repeated subscripts i and j indicate summation, whereas N_n is the number of the shape functions per element. For the numerical assessments in this study, the classical four-node Lagrange (B4) element is employed. Additional information can be found in Bathe [4].

For the continuation of the explanation, it is convenient to define a compact notation for the real and the virtual systems as shown below:

$$u_l = N_i F_{u_l \tau} q_{l_{\tau i}} = \sum_{i=1}^{N_n} \sum_{\tau=1}^{M_{u_l}} N_i F_{u_l \tau} q_{l_{\tau i}} \tag{19}$$

$$\delta u_m = N_j F_{u_m s} \delta q_{m_{sj}} = \sum_{j=1}^{N_n} \sum_{s=1}^{M_{u_m}} N_j F_{u_m s} \delta q_{m_{sj}} \tag{20}$$

where l and m can take the values x, y and z. The summations over i (or j) and τ (or s) have been explicitly written in the previous formulae for the sake of clarity. Furthermore, it is clear that there is no summation over l (or m). This formulation will be useful for the assembly of the matrices of the linear structural system, explained in the following Section 4.

4 | Governing Equations and Finite Element Matrices

In this section, the governing equations are derived by using the novel methodology.

In classical elasticity, the stress tensor, $\boldsymbol{\sigma}$, and strain tensor, $\boldsymbol{\epsilon}$, are conveniently represented in vector form as follows:

$$\boldsymbol{\sigma} = \left\{ \sigma_{xx} \ \sigma_{yy} \ \sigma_{zz} \ \sigma_{yz} \ \sigma_{xz} \ \sigma_{xy} \right\}^T, \quad \boldsymbol{\epsilon} = \left\{ \epsilon_{xx} \ \epsilon_{yy} \ \epsilon_{zz} \ \epsilon_{yz} \ \epsilon_{xz} \ \epsilon_{xy} \right\}^T \tag{21}$$

The geometric relationships between strains and displacements can be defined as:

$$\boldsymbol{\epsilon} = \mathbf{D}\mathbf{u} \tag{22}$$

where **D** represents the matrix of differential operators, applicable in the case of small displacements and angles of rotation:

$$\mathbf{D} = \begin{bmatrix} \partial_x & 0 & 0 \\ 0 & \partial_y & 0 \\ 0 & 0 & \partial_z \\ 0 & \partial_z & \partial_y \\ \partial_z & 0 & \partial_x \\ \partial_y & \partial_x & 0 \end{bmatrix} \tag{23}$$

For the sake of clarity, strains can be expressed in detail using the CUF Equation (15) and FEM Equation (17) approximations as follows;

$$\begin{aligned}
\epsilon_{xx} &= u_{x,x} = \frac{\partial}{\partial x}\left(N_i F_{u_x\tau} q_{x_{\tau i}}\right) = N_i F_{u_x\tau,x} q_{x_{\tau i}} \\
\epsilon_{yy} &= u_{y,y} = \frac{\partial}{\partial y}\left(N_i F_{u_y\tau} q_{y_{\tau i}}\right) = N_{i,y} F_{u_y\tau} q_{y_{\tau i}} \\
\epsilon_{zz} &= u_{z,z} = \frac{\partial}{\partial z}\left(N_i F_{u_z\tau} q_{z_{\tau i}}\right) = N_i F_{u_z\tau,z} q_{z_{\tau i}} \\
\epsilon_{yz} &= u_{y,z} + u_{z,y} = \frac{\partial}{\partial z}\left(N_i F_{u_y\tau} q_{y_{\tau i}}\right) + \frac{\partial}{\partial y}\left(N_i F_{u_z\tau} q_{z_{\tau i}}\right) = N_i F_{u_y\tau,z} q_{y_{\tau i}} + N_{i,y} F_{u_z\tau} q_{z_{\tau i}} \\
\epsilon_{xz} &= u_{x,z} + u_{z,x} = \frac{\partial}{\partial z}\left(N_i F_{u_x\tau} q_{x_{\tau i}}\right) + \frac{\partial}{\partial x}\left(N_i F_{u_z\tau} q_{z_{\tau i}}\right) = N_i F_{u_x\tau,z} q_{x_{si}} + N_i F_{u_z\tau,x} q_{z_{\tau i}} \\
\epsilon_{xy} &= u_{x,y} + u_{y,x} = \frac{\partial}{\partial y}\left(N_i F_{u_x\tau} q_{x_{\tau i}}\right) + \frac{\partial}{\partial x}\left(N_i F_{u_y\tau} q_{y_{\tau i}}\right) = N_{i,y} F_{u_x\tau} q_{x_{\tau j}} + N_i F_{u_y\tau,x} q_{y_{\tau i}}
\end{aligned} \tag{24}$$

The virtual variations of the strains can be easily written with the proposed notation by using Equations (16) and (18).

In this study, linear elastic isotropic materials are considered, leading to the following constitutive relation:

$$\boldsymbol{\sigma} = \mathbf{C}\boldsymbol{\epsilon} \tag{25}$$

where **C** is the matrix of the material coefficients, and it can be written as follows:

$$\mathbf{C} = \begin{bmatrix} C_{11} & C_{12} & C_{13} & 0 & 0 & 0 \\ C_{12} & C_{22} & C_{23} & 0 & 0 & 0 \\ C_{13} & C_{32} & C_{33} & 0 & 0 & 0 \\ 0 & 0 & 0 & C_{55} & 0 & 0 \\ 0 & 0 & 0 & 0 & C_{44} & 0 \\ 0 & 0 & 0 & 0 & 0 & C_{66} \end{bmatrix} \tag{26}$$

For the sake of completeness, the stress components can be written in the followings

$$\begin{aligned}
\sigma_{xx} &= C_{11}\epsilon_{xx} + C_{12}\epsilon_{yy} + C_{13}\epsilon_{zz} \\
\sigma_{yy} &= C_{12}\epsilon_{xx} + C_{22}\epsilon_{yy} + C_{23}\epsilon_{zz} \\
\sigma_{zz} &= C_{13}\epsilon_{xx} + C_{23}\epsilon_{yy} + C_{33}\epsilon_{zz} \\
\sigma_{yz} &= C_{44}\epsilon_{yz} \\
\sigma_{xz} &= C_{55}\epsilon_{xz} \\
\sigma_{xy} &= C_{66}\epsilon_{xy}
\end{aligned} \tag{27}$$

To derive the governing equations for the novel beam FEs, the principle of virtual work is employed, which states:

$$\delta L_{int} = \delta L_{ext} \tag{28}$$

First, the internal work must be taken into account, and its explicit expression is given as follows:

$$\delta L_{int} = \int_V \delta \epsilon^T \boldsymbol{\sigma} \mathrm{d}V = \int_V \left(\delta\epsilon_{xx}\sigma_{xx} + \delta\epsilon_{yy}\sigma_{yy} + \delta\epsilon_{zz}\sigma_{z} + \delta\epsilon_{yz}\sigma_{yz} + \delta\epsilon_{xz}\sigma_{xz} + \delta\epsilon_{xy}\sigma_{xy} \right) \mathrm{d}V \tag{29}$$

where $\mathrm{d}V = \mathrm{d}x\mathrm{d}y\mathrm{d}z$. Using displacement-strain relation Equation (22), the CUF and the FEM approximations Equations (17) and (18), and the constitutive equations Equation (25), it is possible to arrive to the following expression for the internal work:

$$\begin{aligned}
\delta L_{int} = \\
&+ \delta q_{x_{sj}} C_{11} \int_L N_j N_i \mathrm{d}y \int_A F_{u_x s,x} F_{u_x \tau,x} \mathrm{d}x\mathrm{d}z \; q_{x_{\tau i}} + \delta q_{x_{sj}} C_{12} \int_L N_j N_{i,y} \mathrm{d}y \int_A F_{u_x s,x} F_{u_y \tau} \mathrm{d}x\mathrm{d}z \; q_{y_{\tau i}} \\
&+ \delta q_{x_{sj}} C_{13} \int_L N_j N_i \mathrm{d}y \int_A F_{u_x s,x} F_{u_z \tau,z} \mathrm{d}x\mathrm{d}z \; q_{z_{\tau i}} + \delta q_{y_{sj}} C_{12} \int_L N_{j,y} N_i \mathrm{d}y \int_A F_{u_y s} F_{u_x \tau,x} \mathrm{d}x\mathrm{d}z \; q_{x_{\tau i}} \\
&+ \delta q_{y_{sj}} C_{22} \int_L N_{j,y} N_{i,y} \mathrm{d}y \int_A F_{u_y s} F_{u_y \tau} \mathrm{d}x\mathrm{d}z \; q_{y_{\tau i}} + \delta q_{y_{sj}} C_{23} \int_L N_{j,y} N_i \mathrm{d}y \int_A F_{u_y s} F_{u_z \tau,z} \mathrm{d}x\mathrm{d}z \; q_{z_{\tau i}} \\
&+ \delta q_{x_{sj}} C_{66} \int_L N_{j,y} N_{i,y} \mathrm{d}y \int_A F_{u_x s} F_{u_x \tau} \mathrm{d}x\mathrm{d}z \; q_{x_{\tau i}} + \delta q_{y_{sj}} C_{66} \int_L N_j N_{i,y} \mathrm{d}y \int_A F_{u_y s,x} F_{u_x \tau} \mathrm{d}x\mathrm{d}z \; q_{x_{\tau i}} \\
&+ \delta q_{x_{sj}} C_{66} \int_L N_{j,y} N_i \mathrm{d}y \int_A F_{u_z s} F_{u_x \tau,x} \mathrm{d}x\mathrm{d}z \; q_{y_{\tau i}} + \delta q_{y_{sj}} C_{66} \int_L N_j N_i \mathrm{d}y \int_A F_{u_y s,x} F_{u_y \tau,x} \mathrm{d}x\mathrm{d}z \; q_{y_{\tau i}} \\
&+ \delta q_{z_{sj}} C_{44} \int_L N_{j,y} N_{i,y} \mathrm{d}y \int_A F_{u_z s} F_{u_z \tau} \mathrm{d}x\mathrm{d}z \; q_{z_{\tau i}} + \delta q_{y_{sj}} C_{44} \int_L N_j N_{i,y} \mathrm{d}y \int_A F_{u_y s,x} F_{u_z \tau} \mathrm{d}x\mathrm{d}z \; q_{z_{\tau i}} \\
&+ \delta q_{z_{sj}} C_{44} \int_L N_{j,y} N_i \mathrm{d}y \int_A F_{u_z s} F_{u_y \tau,z} \mathrm{d}x\mathrm{d}z \; q_{y_{\tau i}} + \delta q_{y_{sj}} C_{44} \int_L N_j N_i \mathrm{d}y \int_A F_{u_y s,z} F_{u_y \tau,z} \mathrm{d}x\mathrm{d}z \; q_{y_{\tau i}} \\
&+ \delta q_{z_{sj}} C_{55} \int_L N_j N_i \mathrm{d}y \int_A F_{u_z s,x} F_{u_z \tau,z} \mathrm{d}x\mathrm{d}z \; q_{z_{\tau i}} + \delta q_{x_{sj}} C_{55} \int_L N_j N_i \mathrm{d}y \int_A F_{u_x s,z} F_{u_z \tau,x} \mathrm{d}x\mathrm{d}z \; q_{z_{\tau i}} \\
&+ \delta q_{z_{sj}} C_{55} \int_L N_j N_i \mathrm{d}y \int_A F_{u_z s,x} F_{u_x \tau,z} \mathrm{d}x\mathrm{d}z \; q_{x_{\tau i}} + \delta q_{x_{sj}} C_{55} \int_L N_j N_i \mathrm{d}y \int_A F_{u_x s,z} F_{u_x \tau,z} \mathrm{d}x\mathrm{d}z \; q_{x_{\tau i}} \\
&+ \delta q_{z_{sj}} C_{13} \int_L N_j N_i \mathrm{d}y \int_A F_{u_z s,x} F_{u_x \tau,x} \mathrm{d}x\mathrm{d}z \; q_{x_{\tau i}} + \delta q_{z_{sj}} C_{23} \int_L N_j N_{i,y} \mathrm{d}y \int_A F_{u_z s,z} F_{u_y \tau} \mathrm{d}x\mathrm{d}z \; q_{y_{\tau i}} \\
&+ \delta q_{z_{sj}} C_{33} \int_L N_j N_i \mathrm{d}y \int_A F_{u_x s,z} F_{u_z \tau,z} \mathrm{d}x\mathrm{d}z \; q_{z_{\tau i}}
\end{aligned} \tag{30}$$

After having studied the internal work, the external work for point loads is evaluated:

$$\delta L_{ext} = \delta \mathbf{u}^T \mathbf{P} = \left(\delta u_x P_{u_x} + \delta u_y P_{u_y} + \delta u_z P_{u_z} \right) \tag{31}$$

By employing the CUF and FEM approximations for the virtual variations Equation (18), the following expression can be written:

$$\delta L_{ext} = \delta q_{x_{sj}} N_j F_{u_x s} P_{u_x} + \delta q_{y_{sj}} N_j F_{u_y s} P_{u_y} + \delta q_{z_{sj}} N_j F_{u_z s} P_{u_z} \tag{32}$$

In this way, it is possible to obtain three governing equations for each virtual displacement:

$$\begin{aligned}
\delta q_{x_{sj}} &: K_{u_x u_x s\tau ji} q_{x_{\tau i}} + K_{u_x u_y s\tau ji} q_{y_{\tau i}} + K_{u_x u_z s\tau ji} q_{z_{\tau i}} = P_{u_x sj} \\
\delta q_{y_{sj}} &: K_{u_y u_x s\tau ji} q_{x_{\tau i}} + K_{u_y u_y s\tau ji} q_{y_{\tau i}} + K_{u_y u_z s\tau ji} q_{z_{\tau i}} = P_{u_y sj} \\
\delta q_{z_{sj}} &: K_{u_z u_x s\tau ji} q_{x_{\tau i}} + K_{u_z u_y s\tau ji} q_{y_{\tau i}} + K_{u_z u_z s\tau ji} q_{z_{\tau i}} = P_{u_z sj}
\end{aligned} \tag{33}$$

For the sake of completeness, the nine fundamental nuclei of the stiffness matrix are written explicitly in Appendix B.

In this work, the FN of the stiffness matrix is the single scalar $K_{mls\tau ji}$. In this way, the theory consists of nine independent scalar parameters. On the contrary, the previous CUF-based papers used as the kernel a submatrix 3×3. The proposed

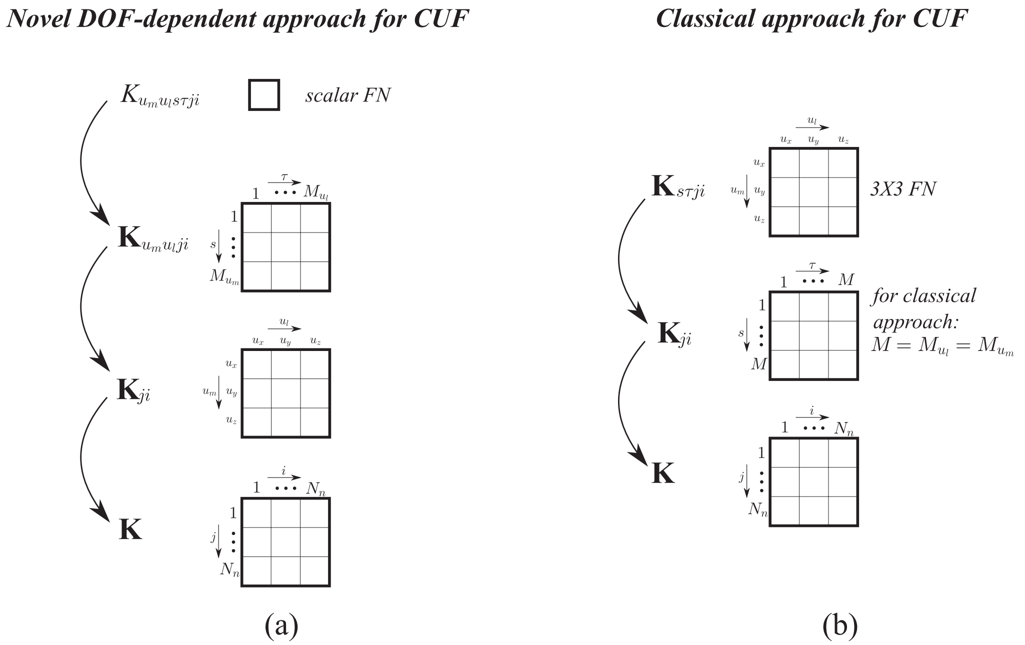

FIGURE 8 | Assembly of the stiffness matrix for the novel approach (a) and classical CUF (b), starting from the fundamental nuclei.

modification permits to individually treat the displacement variable, while in the previous system, all the variables had to use the same expansion theory.

Figure 8 shows the differences between the two methods when assembling the stiffness matrix. In the present method (see Figure 8a), the invariant kernel is expanded on s and τ, then the resultant submatrix is expanded on u_m and u_l, then the resultant submatrix is expanded on j and i, arriving at the structural matrix. On the other hand, in the classical method (see Figure 8b), the loops on the displacement variables are embedded in the 3×3 FN, that is, $K_{u_m u_l}$ is a component of the matrix $\mathbf{K}_{s\tau ji}$. Then, this nucleus is expanded on s and τ, then the resultant submatrix is expanded on j and i, arriving at the structural matrix.

An example will be shown in the following section.

5 | Assembly

This section outlines the process for assembling matrices within the new Unified Formulation context. To illustrate this process, consider the example depicted in Figure 9, which features a two-node beam (B2). The structural theories are also explained in the same figure. The variables u_x and u_y are approximated using a second-order model (TE2), while the first-order model (TE1) is applied to the variable u_z. Consequently, $M_{u_x} = M_{u_y} = 6$ and $M_{u_z} = 3$. This results in 15 DOF for each FE node, leading to a total of 30 DOF for the entire structure. In Figure 10, the stiffness matrix with dimensions of 30×30 and the load vector with dimensions of 30 are illustrated for the entire structure. Each submatrix $\mathbf{K}_{ji}$ is further divided into nine submatrices, while each subvector $\mathbf{P}_j$ consists of three smaller subvectors. For instance, Figure 11 clearly illustrates the nine components of $\mathbf{K}_{11}$ and the three components of $\mathbf{P}_1$. The dimensions and shapes of the matrices $\mathbf{K}_{u_m u_l 11}$ depend on the number of terms in the models used for each displacement variable. For example, $\mathbf{K}_{u_x u_x 11}$, $\mathbf{K}_{u_x u_y 11}$, $\mathbf{K}_{u_x u_y 11}$, and $\mathbf{K}_{u_y u_y 11}$ are square 6×6 matrices, as M_{u_x} and M_{u_y} are both equal to 6. However, $\mathbf{K}_{u_z u_z 11}$ is a square matrix with dimensions of 3×3, corresponding to $M_{u_z} = 3$. The use of different M_{u_l} (and M_{u_m}) for different variables leads to rectangular $\mathbf{K}_{u_m u_l 11}$ matrices with varying dimensions, such as $\mathbf{K}_{u_x u_z 11}$, $\mathbf{K}_{u_y u_z 11}$, $\mathbf{K}_{u_z u_x 11}$, and $\mathbf{K}_{u_z u_y 11}$. For the sake of clarity, in Figure 11, the submatrices $\mathbf{K}_{u_m u_l 11}$ are indicated to as $\mathbf{K}_{u_m u_l}$. In conclusion, each 1×1 $K_{s\tau ji}$ FN corresponds to the real components of the matrices. This procedure can be applied to the load vector.

6 | Numerical Results

In this section, three benchmark cases are examined, focusing on both displacements and stresses. The first case involves a beam with a compact cross-section. Classical theories are compared along with both *uniform* and *reduced* Taylor expansions. The second case study features a hollow square cross-section beam, while the third benchmark evaluates an open

$$
\begin{array}{lll}
\text{TE2:} & u_x = u_{x_1} + x u_{x_2} + z u_{x_3} + x^2 u_{x_4} + xz u_{x_5} + z^2 u_{x_6} & M_{u_x} = 6 \\
\text{TE2:} & u_y = u_{y_1} + x u_{y_2} + z u_{y_3} + x^2 u_{y_4} + xz u_{y_5} + z^2 u_{y_6} & M_{u_y} = 6 \\
\text{TE1:} & u_z = u_{z_1} + x u_{z_2} + z u_{z_3} & M_{u_z} = 3
\end{array}
$$

FIGURE 9 | Example of a beam element. u_x and u_y are studied by using a second-order model, whereas the a complete linear theory approximates the variable u_z.

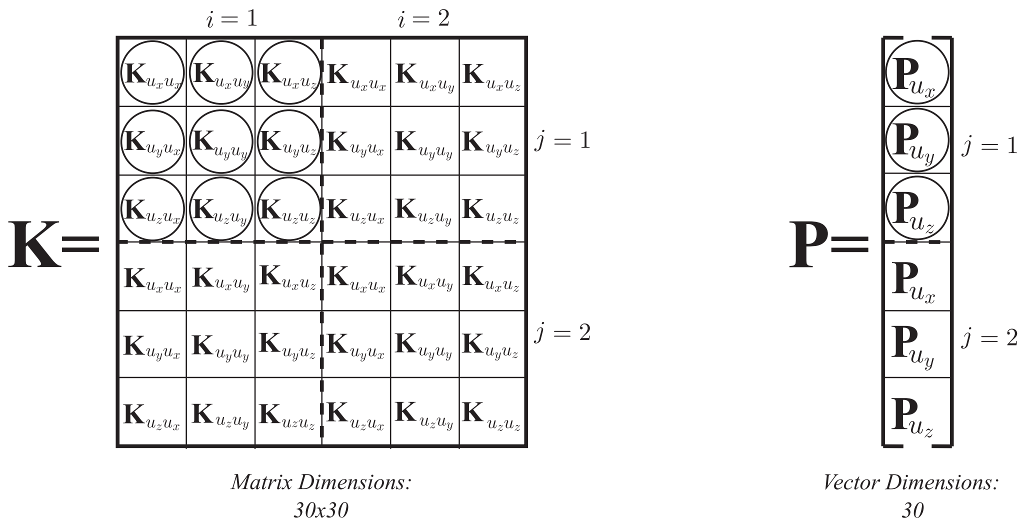

FIGURE 10 | Assembly of the general stiffness matrix and the general load vector.

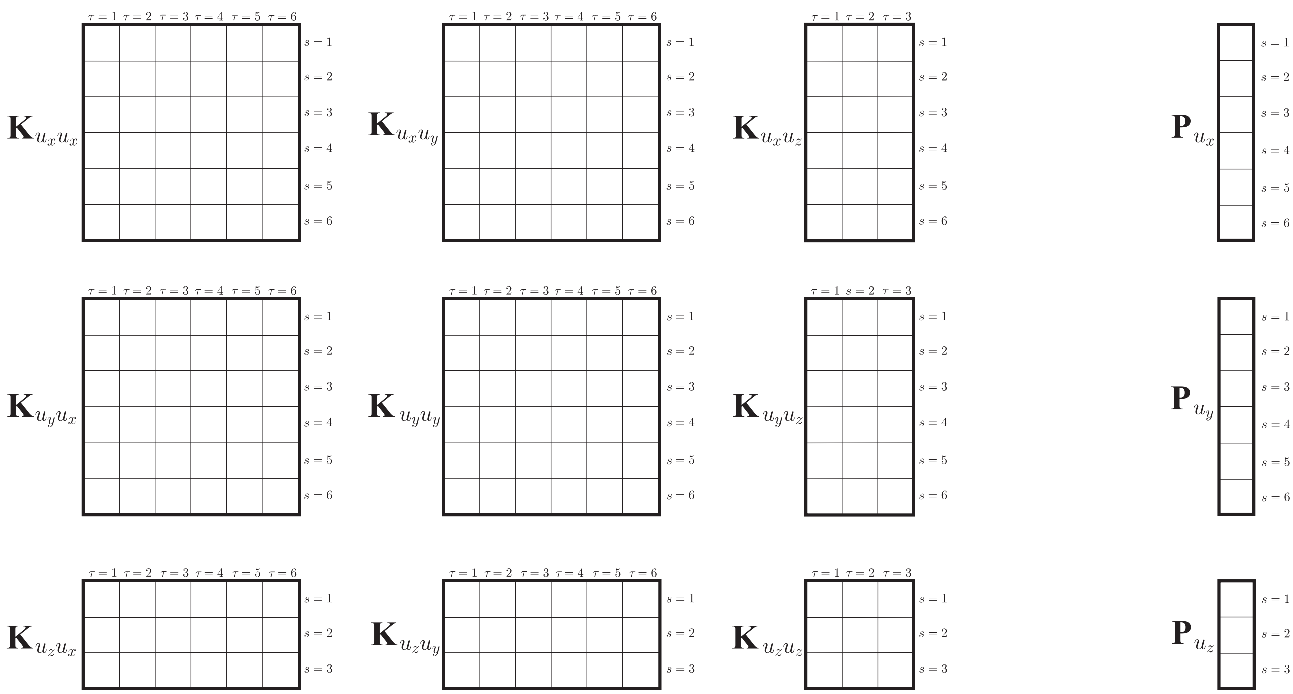

FIGURE 11 | Assembly of the stiffness matrix (here only the submatrix $\mathbf{K}_{11}$ is considered) and the load vector (here only the sub-matrix subvector $\mathbf{P}_1$ is considered).

C-shaped cross-section beam. For these last two examples, *uniform* and *different* theories are both used. In all three cases, point loads and clamped boundary conditions are considered. To alleviate shear locking, the selective reduced integration method is implemented. Throughout these analyses, an illustration of the DOF is provided for the sake of comparison.

For the *uniform* models, they are labeled as TEP, where P denotes the polynomial order. Classical theories are represented with acronyms. When *reduced* models are employed, they are named after the equation where they are defined, for instance, Equation (XX). For *different* theories, a distinct notation is required. In this scenario, the acronym TEP is specified for each displacement variable. As an example, TE2-TE3-TE2 uses a second-order polynomial for u_x and u_z and a third-order theory for u_y.

6.1 | Beam With Compact Sections

The first benchmark involves a cantilevered beam, originally introduced by Carrera and Petrolo [52]. The geometric properties and types of loading conditions are depicted in Figure 12. The analyses account for transverse and torsion loads. The material properties are defined as follows: $E = 75$ [GPa], and $\nu = 0.33$. The beam is clamped at $y = 0$, and the height of the cross-section, denoted as h, is 0.2 [m]. Both slender ($L/h = 100$) and relatively short ($L/h = 10$) beams are considered. In alignment with the reference solution [52], the beam axis is discretized using 40 B4 elements in all cases. The reference solution is established based on a fourth-order Taylor expansion on the cross-section, and it encompasses evaluations of displacements and in-plane stresses. The results are presented as percentage variations relative to the reference solution:

$$\delta_{u_z} = \frac{u_z}{u_z(\text{Ref})} \times 100 \qquad \delta_{u_y} = \frac{u_y}{u_y(\text{Ref})} \times 100 \tag{34}$$

$$\delta_{\sigma_{yy}} = \frac{\sigma_{yy}}{\sigma_{yy}(\text{Ref})} \times 100 \qquad \delta_{\sigma_{xy}} = \frac{\sigma_{xy}}{\sigma_{xy}(\text{Ref})} \times 100 \qquad \delta_{\sigma_{xx}} = \frac{\sigma_{xx}}{\sigma_{xx}(\text{Ref})} \times 100 \tag{35}$$

In this analysis, both uniform Taylor expansions, such as TE2, and reduced structural theories are employed. The definitions of the displacement variables can be found in Appendix C. For the sake of comparison, the number of expansions for each displacement variable, namely M_{ux}, M_{uy}, and M_{u_z} are specified.

6.1.1 | Bending Case

The first loading case considers a concentrated load F_z equal to 50 [N] applied at [0, L, 0], as illustrated in Figure 12a. The transverse displacement, u_z, are computed at [0, L, 0] while the stresses, σ_{yy} and σ_{xx}, are evaluated at [0, 0, $h/2$].

Table 3 presents the results for the slender beam. The linear theories are displayed in the first rows. The vertical displacement is well captured, but the stress components significantly differ from those obtained in the reference solution. TBM

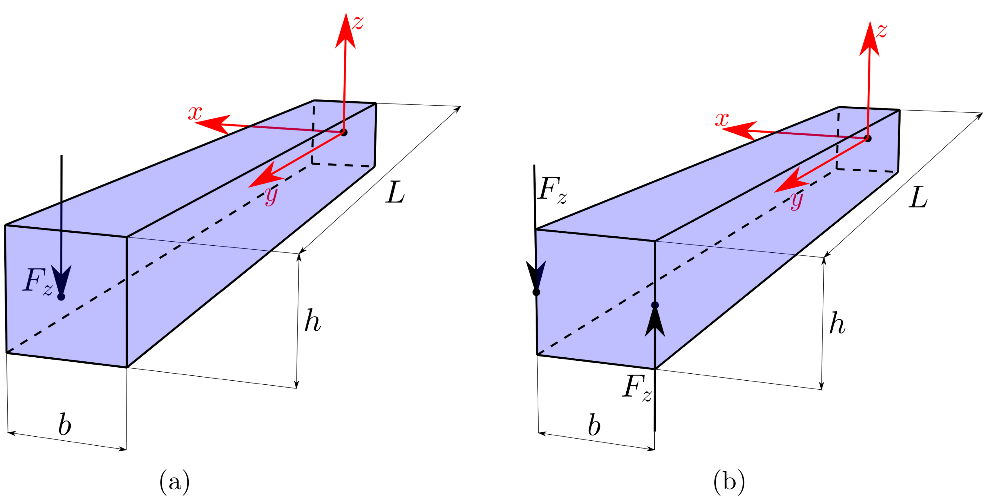

FIGURE 12 | Geometrical properties of the cantilever beam with compact section. The case study is taken from [52]. (a) Transverse Load, (b) Torsion Load.

TABLE 3 | Compact beam, case $L/h = 100$. Loading case: bending.

Model	$M_{u_x}/M_{u_y}/M_{u_z}$	$\delta^a_{u_z}$ [%]	$\delta^b_{\sigma_{yy}}$ [%]	$\delta^b_{\sigma_{xx}}$ [%]	DOF
First order (Poisson locking correction)					
TE1	3/3/3	100.2	88.1	130.5	1089
TBM	1/3/1	100.2	88.1	130.5	605
Equation (51)	0/1/1	100.2	88.1	130.5	242
Second order					
TE2	6/6/6	99.99	100.7	100.7	2178
Equation (52)	1/1/2	97.04	100.1	100.1	484
Third order					
TE3	10/10/10	100	100	100	3630
Equation (53)	1/3/2	97.1	99.9	99.9	726
Fourth order					
TE4 [52]	15/15/15	100	100	100	5445
Equation (54)	3/3/5	99.5	100	100	1331

(a): Computed at $[0, L, 0]$; (b): Computed at $[0, 0, h/2]$

is also shown. However, u_{z_1} and zu_{y_1} are sufficient to provide non-null solutions (as described in Equation (51)), where $M_{u_x} = 0$, $M_{u_y} = 1$, and $M_{u_z} = 1$. Using a kinematics model based on only these two displacement variables yields the same results as the full linear model at the considered points. This result is well-documented and arises from the symmetry of the geometry and the loading conditions, as noted in Washizu [15]. Subsequently, the relevant second-order terms are investigated. Full and a reduced model (as specified in Equation (52)) are employed, focusing only on the significant quadratic contributions. The full second-order model demonstrates remarkable accuracy in matching the fourth-order results. The effective terms encompass xzu_{x_1} and $z^2u_{z_2}$, with a total of $M_{u_x} = 1$, $M_{u_y} = 1$, and $M_{u_z} = 2$. Finally, analyses for the third- and fourth-order terms are conducted. As observed for the previous cases, there is a substantial reduction in the total number of effective terms compared to the full expansion cases. Equation (53) (with $M_{u_x} = 1$, $M_{u_y} = 3$, and $M_{u_z} = 2$) and Equation (54) (with $M_{u_x} = 3$, $M_{u_y} = 3$, and $M_{u_z} = 5$) represent the reduced models for the third- and fourth-order expansions, respectively.

Table 4 presents the results for the short beam, utilizing the same theories as in the slender case. The variations in the solution provided by the higher-order terms are more significant than in the case of a slender beam. Nevertheless, the same conclusions can be drawn as in the slender beam.

Finally, a comparison between three CUF-based models, three classical beam models (B31, B32, and B33), a refined solid model (C3D20R), and the analytical Euler-Bernoulli theory [2] for the short beam ($L/h = 10$) is shown in Table 5. The formula for calculating the maximum transverse displacement and axial stresses is:

$$u_z = \frac{F_z\, L}{3\, E\, I} \qquad \sigma_{yy} = \frac{F_z\, Lh/2}{I} \tag{36}$$

being I the bending moment of inertia. Forty FEs are employed for each ABAQUS model, while a 3D $5 \times 50 \times 5$ mesh is used for the solid model. The results are illustrated in the central columns, while DOFs and the computational times are given in the last two columns. The results clearly demonstrate that the proposed models outperform the commercial ones in terms of efficiency. Different from the analytical and beam ABAQUS models, the stress component σ_{xx} can be calculated even from the Model described in Equation (51), which features only two DOFs per node.

6.1.2 | Torsion Case

In the second loading case, two concentrated opposite forces, F_y, are applied at $[\pm b/2, L, 0]$, as depicted in Figure 12b. The magnitudes of the forces are 250 [kN]. The transverse and axial displacements are computed at $[-b/2, L, -h/2]$, and the

TABLE 4 | Compact beam, case $L/h = 10$. Loading case: bending.

Model	$M_{u_x}/M_{u_y}/M_{u_z}$	$\delta^a_{u_z}$ [%]	$\delta^b_{\sigma_{yy}}$ [%]	$\delta^b_{\sigma_{xx}}$ [%]	DOF
First order (Poisson locking correction)					
TE1	3/3/3	100.7	87.3	129.2	1089
TBM	1/3/1	100.7	87.3	129.2	605
Equation (51)	0/1/1	100.7	87.3	129.2	242
Second order					
TE2	6/6/6	99.7	89.6	89.1	2178
Equation (52)	1/1/2	96.7	89.6	89.6	484
Third order					
TE3	10/10/10	99.9	97.5	97.5	3630
Equation (53)	1/3/2	97.1	98.5	98.5	726
Fourth order					
TE4 [52]	15/15/15	100	100	100	5445
Equation (54)	3/3/5	99.5	100	100	1331

(a): Computed at $[0, L, 0]$; (b): Computed at $[0, 0, h/2]$

TABLE 5 | Compact beam, case $L/h = 10$. Loading case: bending. Comparison with classical models.

Model	$\delta^a_{u_z}$ [%]	$\delta^b_{\sigma_{yy}}$ [%]	$\delta^b_{\sigma_{xx}}$ [%]	DOF	Time [s]
Present model					
Equation (51)	100.7	87.3	129.2	242	2
Equation (54)	99.5	100	100	1331	4
TE4 [52]	100	100	100	5445	20
Beam ABAQUS models					
B31	100.9	86.1	0.0	246	24
B32	100.9	87.3	0.0	486	24
B33	100.1	87.3	0.0	326	24
Solid ABAQUS model					
C3D20R	100.2	98.3	95.2	20382	36
Analytical model					
Euler [2]	100.1	87.3	0.0	—	—

(a): Computed at $[0, L, 0]$; (b): Computed at $[0, 0, h/2]$

in-plane stress, σ_{xy}, at $[0, 0, h/2]$. The results for the slender and the short beams are shown in Tables 6 and 7, respectively. Also, an analytical model [60] and a refined $6 \times 50 \times 5$ solid model (C3D20R) are listed for the short case. The formula for calculating the maximum transverse displacement and axial stresses is:

$$u_z = \frac{F_z\ b^2 L}{2\ G\ \ 0.1406 b^4} \qquad \sigma_{xy} = \frac{F_z\ b^2}{2\ 0.1406 b^4} \tag{37}$$

being G the shear modulus. In this case, the warping is not considered. Additionally, Figure 13 provides a contour plot for the case $L/h = 10$, illustrating the magnitude of displacements. Three models are compared: TE4, and Equation (61), and Equation (55). The contour plot for TE4 is presented in this paper.

TABLE 6 | Compact beam, case $L/h = 100$. Loading case: torsion.

Model	$M_{u_x}/M_{u_y}/M_{u_z}$	$\delta^a_{u_z}$ [%]	$\delta^a_{u_y}$ [%]	$\delta^b_{\sigma_{xy}}$ [%]	DOF
First order (Poisson locking correction)					
TE1	3/3/3	84.5	0.0	90.9	1089
TBM	1/3/1	0.0	0.0	0.0	605
Equation (55)	1/0/1	84.5	0.0	90.9	242
Second order					
TE2	6/6/6	84.5	123.9	90.9	2178
Equation (56)	4/3/4	84.5	123.9	90.9	1331
Equation (57)	1/1/1	84.5	123.9	90.9	363
Third order					
TE3	10/10/10	84.5	89.1	90.9	3630
Equation (58)	5/5/5	84.5	89.1	90.9	1815
Equation (59)	3/1/3	84.5	89.1	90.9	847
Fourth order					
TE4 [52]	15/15/15	100	100	100	5445
Equation (60)	8/6/8	100	100	100	2662
Equation (61)	3/3/3	100	100	100	1089

(a): Computed at $[-b/2, L, -h/2]$; (b): Computed at $[0, 0, h/2]$

TABLE 7 | Compact beam, case $L/h = 10$. Loading case: torsion.

Model	$M_{u_x}/M_{u_y}/M_{u_z}$	$\delta^a_{u_z}$ [%]	$\delta^a_{u_y}$ [%]	$\delta^b_{\sigma_{xy}}$ [%]	DOF
First order (Poisson locking correction)					
TE1	3/3/3	84.5	0.0	85.1	1089
TBM	1/3/1	0.0	0.0	0.0	605
Equation (55)	1/0/1	84.5	0.0	85.1	242
Second order					
TE2	6/6/6	85.7	131.6	85.1	2178
Equation (56)	4/3/4	85.7	131.6	85.1	1331
Equation (57)	1/1/1	85.7	131.6	85.1	363
Third order					
TE3	10/10/10	85.3	116.2	85.1	3630
Equation (58)	5/5/5	85.3	116.2	85.1	1815
Equation (59)	3/1/3	85.3	116.2	85.1	847
Fourth order					
TE4 [52]	15/15/15	100	100	100	5445
Equation (60)	8/6/8	100	100	100	2662
Equation (61)	3/3/3	100	100	100	1089
Solid ABAQUS model					
C3D20R	—	98.08	81.47	110	27699
Analytical model					
Higdon et al. [60]	—	98.79	0.0	100.9	—

(a): Computed at $[-b/2, L, -h/2]$; (b): Computed at $[0, 0, h/2]$

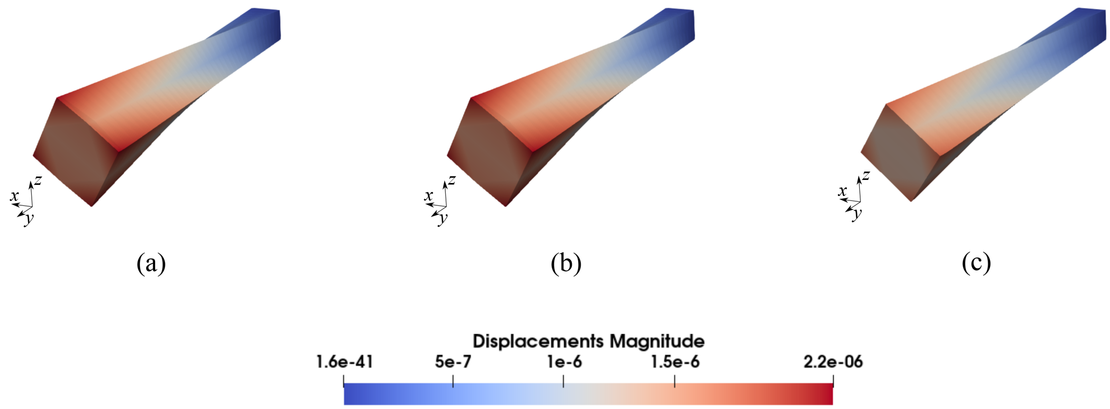

FIGURE 13 | Compact beam, case $L/h = 10$. Loading case: torsion. Contour plot. (a) TE4, (b) Equation (61), (c) Equation (55).

It is interesting to note that in Equation (55), the model demonstrates the same level of accuracy as the TE1 model. However, the TBM fails in evaluating the torsion of the beam, since the two linear terms in Equation (55) are not considered. It is important to emphasize that the analysis of the beam warping is only possible when retaining a second-order term, specifically xzu_{x_1}. Finally, considering the fourth-order models, the total number of effective displacement variables is 9, while the complete set of TE4 has 45 terms. The kinematics model, which is not affected by L/h, is Equation (61). The effect of the span-to-height ratio has a significant impact on the transverse displacement variations δ_{u_z}.

When comparing Equation (54) with Equation (61), it becomes evident that the kinematics model undergoes significant changes with variations in the loading case.

Finally, the best results for the short beam are in good agreement with the solid and closed-form models.

6.2 | Beams With Thin-Walled Closed Cross-Section

A hollow square cross-section is studied as the second benchmark. This case study is taken from [42]. The cross-section geometry and the loading conditions are depicted in Figure 14. The length-to-height ratio, L/h, is set to 20. The height, h, and the width, b, are both equal to 1 [m]. The height-to-thickness ratio, h/t, is equal to 10. Both ends of the beam are clamped. Two point loadings ($F_z = \pm 1[N]$) are applied at $[0, L/2, \mp h/2]$. As for the reference solution [42], ten B4 elements are employed to discretize the beam axis. The reference solution is based on a *uniform* eleven-order Taylor expansion (TE11-TE11-TE11) on the cross-section, allowing to explore higher-order phenomena. The focus is on the evaluation of transverse displacements, u_z. The relative error is quantified using the following expression:

$$\text{err} = \left\| \frac{u_z(\text{Ref}) - u_z}{u_z(\text{Ref})} \right\| \times 100 \tag{38}$$

The DOF reduction is calculated by the following formula:

$$\text{DOF reduction} = \left\| \frac{\text{DOF(Ref)} - \text{DOF}}{\text{DOF(Ref)}} \right\| \times 100 \tag{39}$$

Table 8 displays the vertical displacement, u_z, at the point located at $[0, L/2, -h/2]$. The first three columns specify the model used for each displacement variable. The fifth column presents the relative error. Finally, the table includes the DOF and the DOF Reduction in the last columns. Both *uniform* and *different* models are employed. For the central rows, it is easier to study the models by considering the influence of the order on each displacement component. It is worth noting that for each category, two fixed models, TE8 and TE11, are utilized, while the variable models consist of TE2, TE4, and TE6.

Figure 15 presents a contour plot at the mid-section for the reference solution and three *different* theories: TE2-TE11-TE11, TE11-TE2-TE11, and TE11-TE11-TE2. Among these theories, TE11-TE2-TE11, where a lower polynomial approximates the axial displacement, yields the best results.

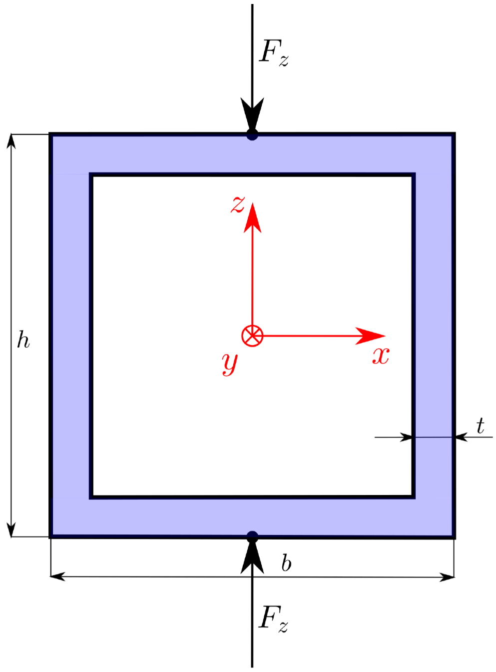

FIGURE 14 | Geometrical properties of the hollow square cross-section. The study case is taken from [42].

TABLE 8 | Hollow square beam. Transverse displacements evaluated in $[0, L/2, -h/2]$.

Model u_x	**Model u_y**	**Model u_z**	**$u_z \times 10^9$ [m]**	**Err[%]**	**DOF**	**DOF reduction [%]**
Literature [42]						
TE11	TE11	TE11	1.270	—	7254	—
Uniform models						
TE2	TE2	TE2	0.0417	96.72	558	92.31
TE4	TE4	TE4	0.178	85.98	1395	80.77
TE6	TE6	TE6	0.739	41.81	2604	64.10
TE8	TE8	TE8	1.046	17.64	4185	42.31
Different models (Influence on u_x)						
TE2	TE8	TE8	0.228	82.05	2976	58.97
TE4	TE8	TE8	0.387	69.53	3255	55.13
TE6	TE8	TE8	0.887	30.16	3658	49.57
TE2	TE11	TE11	0.247	80.55	5022	30.77
TE4	TE11	TE11	0.421	66.85	5301	26.92
TE6	TE11	TE11	0.991	21.97	5704	21.37
Different models (Influence on u_y)						
TE8	TE2	TE8	0.581	54.25	2976	58.97
TE8	TE4	TE8	0.687	45.91	3255	55.13
TE8	TE6	TE8	0.970	23.62	3658	49.57
TE11	TE2	TE11	0.685	46.06	5022	30.77
TE11	TE4	TE11	0.824	35.12	5301	26.92
TE11	TE6	TE11	1.134	10.71	5704	21.37
Different models (Influence on u_z)						
TE8	TE8	TE2	0.0474	96.27	2976	58.97
TE8	TE8	TE4	0.245	80.71	3255	55.13
TE8	TE8	TE6	0.862	32.13	3658	49.57
TE11	TE11	TE2	0.0476	96.25	5022	30.77
TE11	TE11	TE4	0.256	79.84	5301	26.92
TE11	TE11	TE6	0.930	26.77	5704	21.37

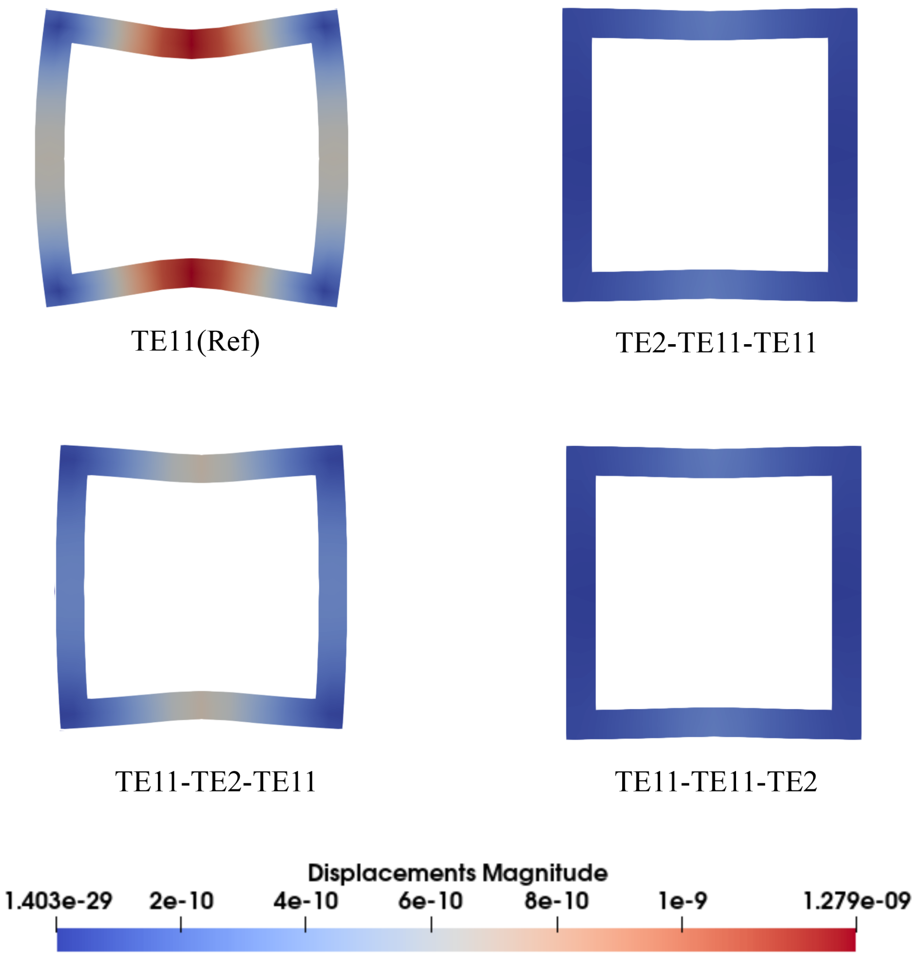

FIGURE 15 | Hollow square beam. Contour plot.

Figure 16 compares the relative error for different theories based on the number of DOFs. Specifically, Figure 16a features models with TE8 fixed for two displacement variables, while Figure 16b showcases models with TE11 fixed for two displacement variables. In both figures, the square symbol represents changes in the u_x model, the star symbol denotes changes in the u_y model, and the circle symbol indicates changes in the u_z model. Within each graph, three groups of models with the same DOFs are shown.

Several important observations can be made based on the results:

- The analysis highlights the necessity for refined models to achieve results that closely match the reference solution.
- Notably, the problem exhibits less sensitivity to the model for u_y. In fact, with the same DOFs, the relative error decreases. Conversely, to attain accurate results, it is essential to retain more terms in models for u_x and u_z.

6.3 | Open C-Shaped Cross-Section

Finally, a cantilevered C-section beam is studied. The cross-section geometry is shown in Figure 17. The length-to-height ratio, L/h, is equal to 20. The height-to-thickness ratio, h/t, is as high as 10 with h and b_2 equal to 1 [m], and b_1 as high as $b_2/2$. Two point loads are applied at $[0, L, \pm 0.4]$, and their magnitudes are as high as ∓ 1 [N]. To be consistent with the reference paper [42], ten B4 elements are used to discretize the beam axis. Also, in this benchmark, the reference solution is based on an eleven-order Taylor expansion on the cross-section to account for the higher-order phenomena. Transverse displacements, u_z, are calculated in the following analyses. The relative error and the DOF reduction are evaluated by Equations (38) and (39), respectively.

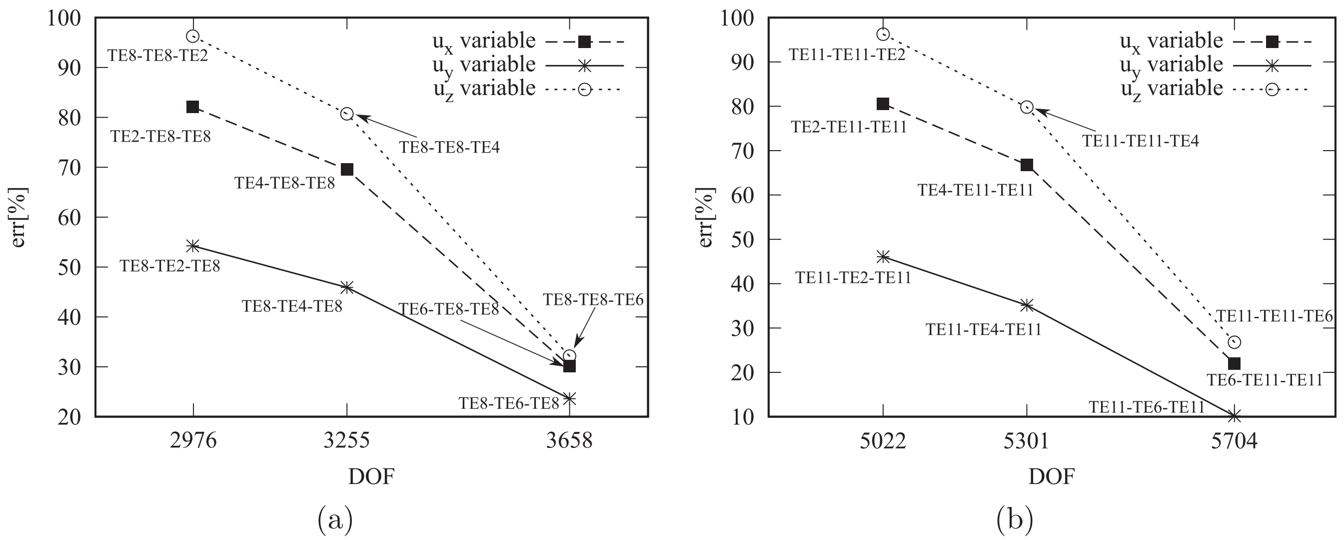

FIGURE 16 | Hollow square beam. Relative error for several models as a function of degrees of freedom. (a) Maximum theory: TE8, (b) Maximum theory: TE11.

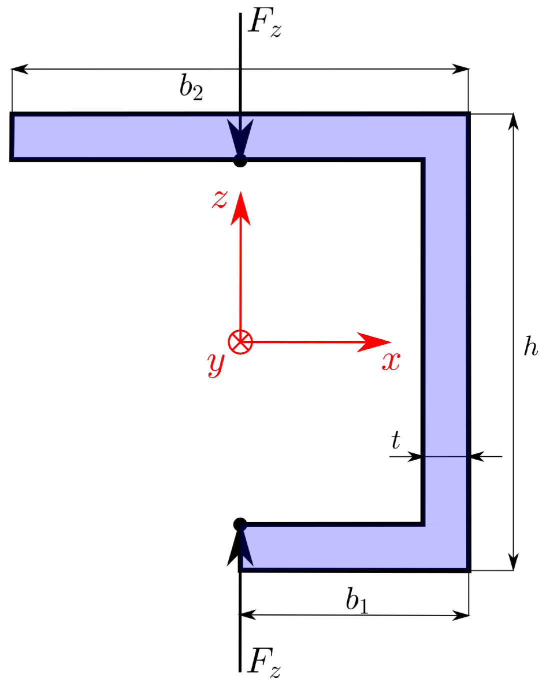

FIGURE 17 | Geometrical properties of the open C-shaped cross-section. The study case is taken from [42].

Table 9 presents the vertical displacement, u_z, at the point located at $[-b_2/2, L, +0.4]$. The table structure mirrors that of the Hollow Square cross-section benchmark. It includes columns specifying the models used for each displacement variable and provides information on relative error, DOFs, and DOF Reduction to facilitate a comprehensive comparison between the various theories. In the following analyses, both *uniform* and *different* models are adopted. Similar to the previous benchmark, the *different* models are categorized into the three groups detailed in Table 9.

In Figure 18, the contour plots at the tip section of three *different* theories, namely TE2-TE11-TE11, TE11-TE2-TE11, and TE11-TE11-TE2, are compared with that of the uniform reference solution.

Figure 19 compares the relative error for various theories as a function of the DOFs. Specifically, Figure 19a presents models where TE8 is fixed for two displacement variables, while Figure 19b depicts models where TE11 is fixed for two displacement variables. The symbols in the graphs have the same meaning as in the previous benchmark.

TABLE 9 | Open C-shaped cross-section. Transverse displacements evaluated in $[-b_2/2, L, +0.4]$.

Model u_x	Model u_y	Model u_z	$-u_z \times 10^8$ [m]	Err[%]	DOF	DOF reduction [%]
Literature [42]						
TE11	TE11	TE11	2.565	—	7254	—
Uniform models						
TE2	TE2	TE2	0.01631	100.6	558	92.31
TE4	TE4	TE4	0.2446	90.46	1395	80.77
TE6	TE6	TE6	1.444	43.66	2604	64.10
TE8	TE8	TE8	2.160	15.72	4185	42.31
Different models (Influence on u_x)						
TE2	TE8	TE8	1.634	36.25	2976	58.97
TE4	TE8	TE8	1.861	27.38	3255	55.13
TE6	TE8	TE8	1.997	22.05	3658	49.57
TE2	TE11	TE11	1.865	27.21	5022	30.77
TE4	TE11	TE11	2.096	18.20	5301	26.92
TE6	TE11	TE11	2.316	9.643	5704	21.37
Different models (Influence on u_y)						
TE8	TE2	TE8	0.5429	78.81	2976	58.97
TE8	TE4	TE8	1.698	33.73	3255	55.13
TE8	TE6	TE8	1.967	23.26	3658	49.57
TE11	TE2	TE11	0.6209	75.77	5022	30.77
TE11	TE4	TE11	1.968	23.20	5301	26.92
TE11	TE6	TE11	2.275	11.24	5704	21.37
Different models (Influence on u_z)						
TE8	TE8	TE2	0.01819	99.29	2976	58.97
TE8	TE8	TE4	0.2993	88.32	3255	55.13
TE8	TE8	TE6	1.793	30.04	3658	49.57
TE11	TE11	TE2	0.01804	99.30	5022	30.77
TE11	TE11	TE4	0.3204	87.50	5301	26.92
TE11	TE11	TE6	1.954	27.73	5704	21.37

The analyses yield the following conclusions:

- The analysis shows that refined models are needed to obtain results close to the reference solution.
- As can be noted, the problem is less dependent on the model u_x. In fact, with the same DOF, the relative error diminishes. On the contrary, more terms in model u_z must be retained to obtain good results.

7 | Conclusions

In this paper, a novel approach to constructing beam theories has been introduced by modifying the CUF and changing the procedure for the assembly of FE matrices. This approach allows for the development of independent structural theories for each variable, enabling the creation of one-dimensional FE models tailored to study various structures. The present work is the first of a series of papers to arrive at a method for the determination of the best theories. Three case studies have been conducted, all drawn from open literature, including compact sections, hollow square sections, and open section

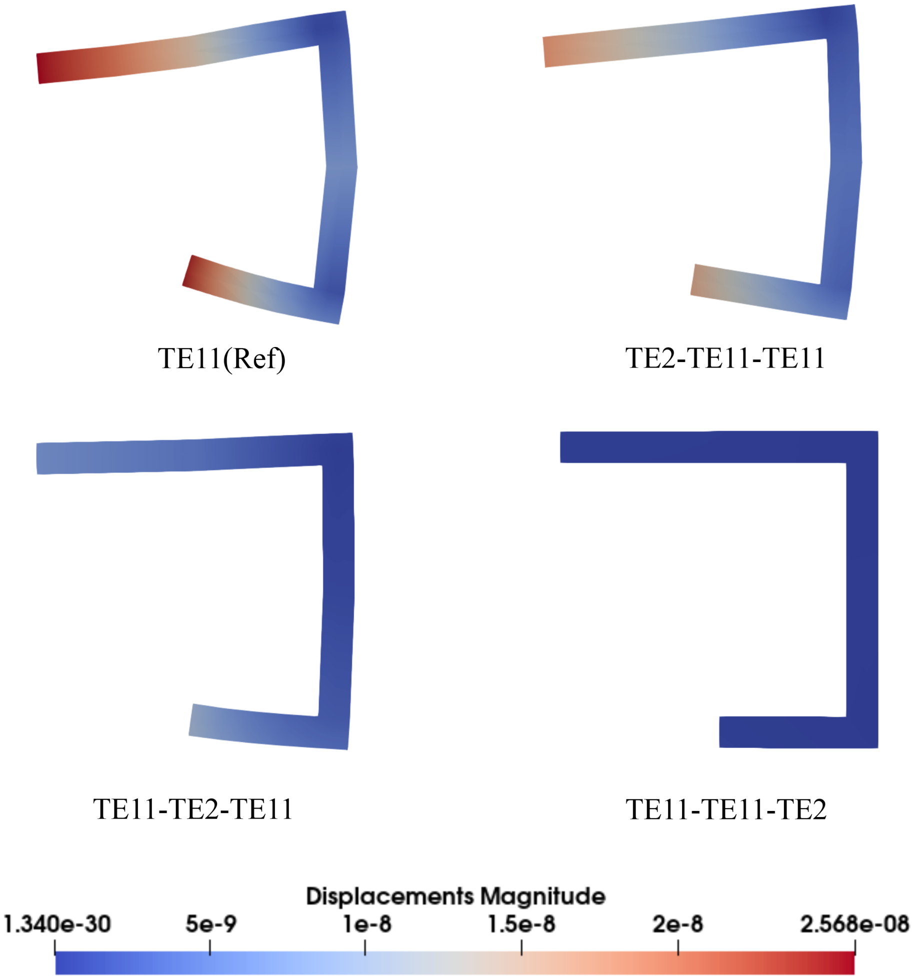

FIGURE 18 | Open C-shaped cross-section. Contour plot.

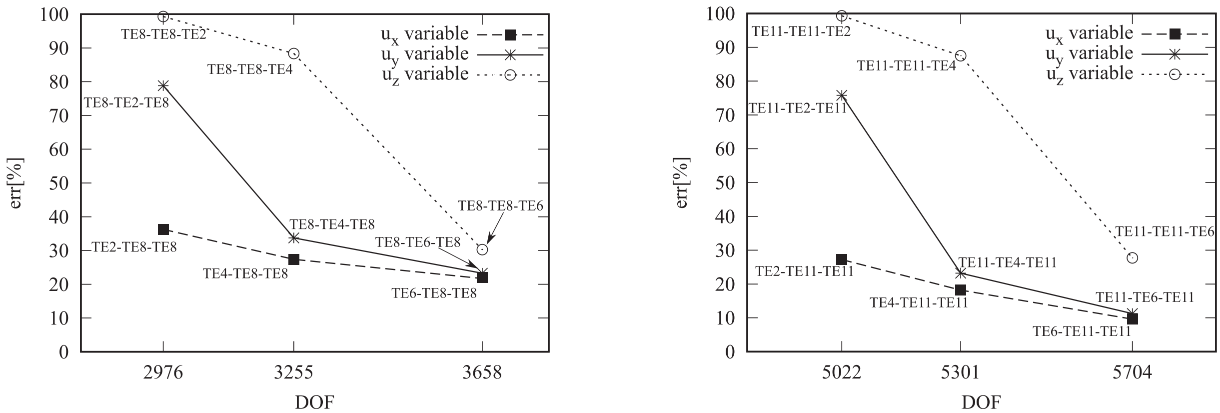

(a) Maximum theory: TE8 (b) Maximum theory: TE11

FIGURE 19 | Open C-shaped cross-section. Relative error for several models as a function of degrees of freedom. (a) Maximum theory: TE8, (b) Maximum theory: TE11.

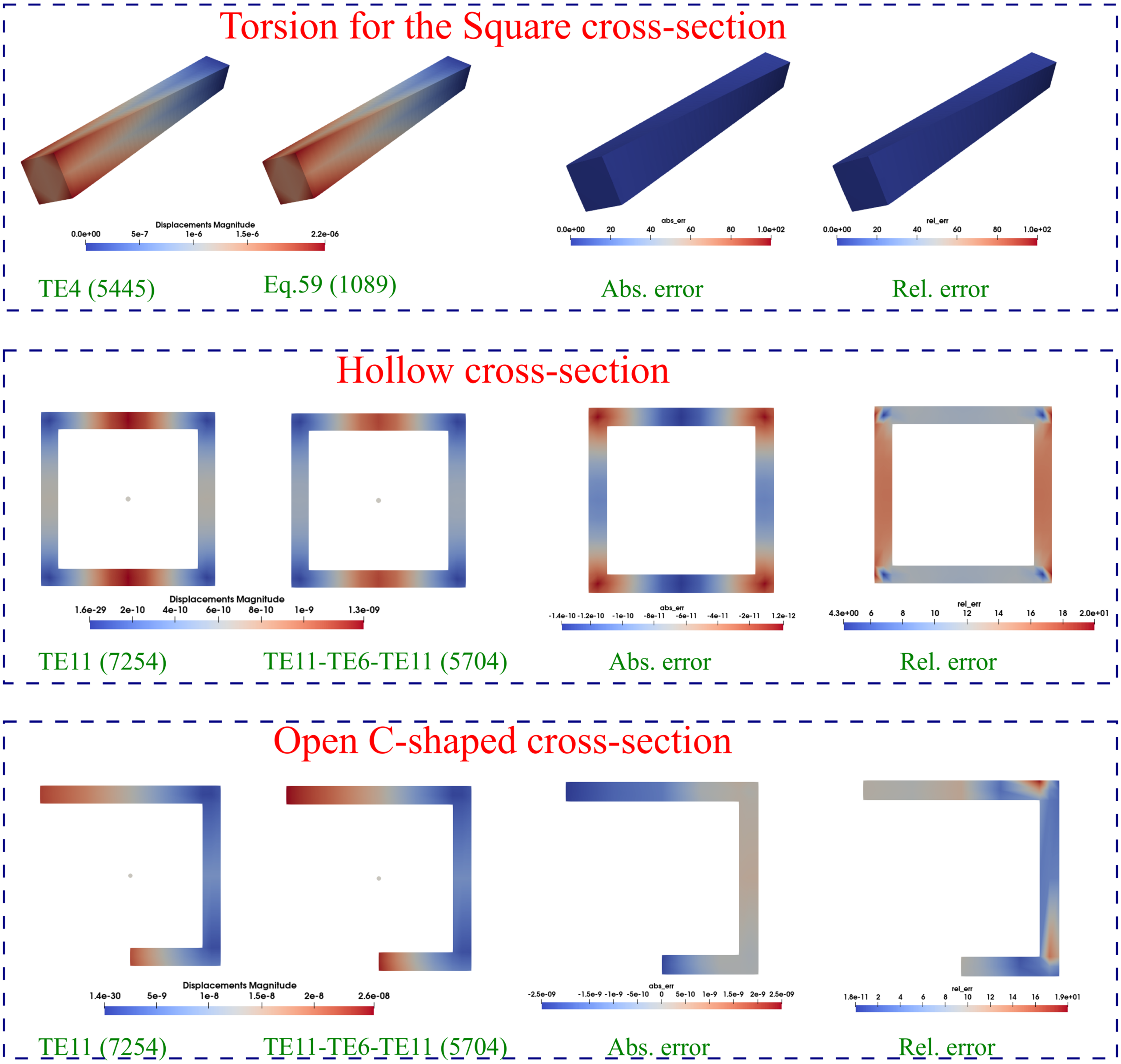

FIGURE 20 | Some results obtained during the present analyses for three different cases. DOF are listed in parentheses. The displacement magnitude is calculated as $displ = \sqrt{u_x^2 + u_y^2 + u_z^2}$, the absolute and relative errors are evaluated as $abs.\ error = displ - displ(\text{Ref})$, $rel.\ err = \left\|\frac{displ(\text{Ref}) - displ}{displ(\text{Ref})}\right\| \times 100$, respectively.

beams, all within the context of isotropic materials and clamped boundary conditions. Figure 20 resumes some of the most interesting outcomes of the work, comparing *uniform* and *reduced* (or *different*) models. Also, the contour plots of absolute and relative errors with respect to the reference solutions are illustrated. The results have been compared with existing literature solutions, leading to the following conclusions:

- It is feasible to significantly reduce computational costs by selectively utilizing only the most relevant terms within the structural theories;
- The choice of the appropriate kinematics model is contingent upon the cross-section geometry and the specific loading conditions;
- The number of effective variables is highly dependent on the nature of the problem under consideration;
- The choice of the models also depends on the desired outcome (e.g., displacements or stresses).

Furthermore, future research efforts could explore the application of our approach to more complex structures, such as plates and shells. Additionally, the extension of this method to multi-field analyses, including thermoelastic or piezoelastic studies, offers promising avenues for further investigation.

Data Availability Statement

The data that support the findings of this study are available from the corresponding author upon reasonable request.

Acknowledgments

Open access publishing facilitated by Politecnico di Torino, as part of the Wiley - CRUI-CARE agreement.

References

1. E. Carrera and E. Zappino, "One-Dimensional Finite Element Formulation With Node-Dependent Kinematics," *Computers & Structures* 192 (2017): 114–125.

2. L. Euler, *Methodus Inveniendi Lineas Curvas Maximi Minimive Proprietate Gaudentes Sive Solutio Problematis Isoperimetrici Latissimo Sensu Accepti*, vol. 1 (Springer Science & Business Media, 1952).

3. S. P. Timoshenko, "On the Transverse Vibrations of Bars of Uniform Cross Section," *Philosophical Magazine* 43 (1922): 125–131.

4. K. J. Bathe, *Finite Element Procedure* (Prentice hall, 1996).

5. J. H. Argyris, "Matrix Analysis of Three-Dimensional Elastic Media - Small and Large Displacements," *AIAA Journal* 3, no. 1 (1965): 45–51.

6. K. J. Bathe and L. W. Ho, "Some Results in the Analysis of Thin Shell Structures," in *Nonlinear Finite Element Analysis in Structural Mechanics*, ed. W. Wunderlich, E. Stein, and K. J. Bathe (Springer, 1981), 122–150.

7. K. S. Surana, "Transition Finite Elements for Three-Dimensional Stress Analysis," *International Journal for Numerical Methods in Engineering* 15, no. 7 (1980): 991–1020.

8. K. S. Surana, "Geometrically Non-Linear Formulation for the Three Dimensional Solid-Shell Transition Finite Elements," *Computers & Structures* 15, no. 5 (1982): 549–566.

9. T. C. Gmür and R. H. Kauten, "Three-Dimensional Solid-To-Beam Transition Elements for Structural Dynamics Analysis," *International Journal for Numerical Methods in Engineering* 36, no. 9 (1993): 1429–1444.

10. A. K. Noor, "Global-Local Methodologies and Their Application to Nonlinear Analysis," *Finite Elements in Analysis and Design* 2, no. 4 (1986): 333–346.

11. V. V. Novozhilov, *Theory of Elasticity* (Pergamon, 1961).

12. R. K. Kapania and S. Raciti, "Recent Advances in Analysis of Laminated Beams and Plates. Part I: Shear Effects and Buckling," *AIAA Journal* 27, no. 7 (1989): 923–935.

13. R. K. Kapania and S. Raciti, "Recent Advances in Analysis of Laminated Beams and Plates. Part II: Vibrations and Wave Propagation," *AIAA Journal* 27, no. 7 (1989): 935–946.

14. E. Carrera, A. Pagani, M. Petrolo, and E. Zappino, "Recent Developments on Refined Theories for Beams With Applications," *Mechanical Engineering Reviews* 2, no. 2 (2015): 1400298.

15. K. Washizu, *Variational Methods in Elasticity and Plasticity* (Pergamon, 1968).

16. V. Z. Vlasov, *Thin-Walled Elastic Beams* (National Technical Information Service, 1984).

17. P. O. Friberg, "Beam Element Matrices Derived From Vlasov's Theory of Open Thin-Walled Elastic Beams," *International Journal for Numerical Methods in Engineering* 21, no. 7 (1985): 1205–1228.

18. R. D. Ambrosini, J. D. Riera, and R. F. Danesi, "A Modified Vlasov Theory for Dynamic Analysis of Thin-Walled and Variable Open Section Beams," *Engineering Structures* 22, no. 8 (2000): 890–900.

19. I. Mechab, N. El Meiche, and F. Bernard, "Analytical Study for the Development of a New Warping Function for High Order Beam Theory," *Composites Part B: Engineering* 119 (2017): 18–31.

20. R. Schardt, "Eine Erweiterung der Technischen Biegetheorie zur Berechnung prismatischer Faltwerke," *Der Stahlbau* 35 (1966): 161–171.

21. M. Ganapathi, B. P. Patel, O. Polit, and M. Touratier, "A C^1 Finite Element Including Transverse Shear and Torsion Warping for Rectangular Sandwich Beams," *International Journal for Numerical Methods in Engineering* 45, no. 1 (1999): 47–75.

22. M. Levinson, "A New Rectangular Beam Theory," *Journal of Sound and Vibration* 74, no. 1 (1981): 81–87.

23. P. R. Heyliger and J. N. Reddy, “A Higher Order Beam Finite Element for Bending and Vibration Problems,” *Journal of Sound and Vibration* 126, no. 2 (1988): 309–326.

24. T. Kant and B. S. Manjunath, “Refined Theories for Composite and Sandwich Beams With C< i >< /i>° Finite Elements,” *Computers & Structures* 33 (2014): 755–764.

25. T. Kant and B. S. Manjunatha, “Higher-Order Theories for Symmetric and Unsymmetric Fiber Reinforced Composite Beams With C< i >< /i>° Finite Elements,” *Finite Elements in Analysis and Design* 6, no. 4 (1990): 303–320.

26. B. S. Manjunatha and T. Kant, “Different Numerical Techniques for the Estimation of Multiaxial Stresses in Symmetric/Unsymmetric Composite and Sandwich Beams With Refined Theories,” *Journal of Reinforced Plastics and Composites* 12, no. 1 (1993): 2–37.

27. B. S. Mallikarjuna and T. Kant, “A Critical Review and Some Results of Recently Developed Refined Theories of Fiber-Reinforced Laminated Composites and Sandwiches,” *Composite Structures* 23, no. 4 (1993): 293–312.

28. R. Kapania and V. Goyal, “Free Vibration of Uncertain Unsymmetrically Laminated Beams,” in *Proceedings of the 19th AIAA Applied Aerodynamics Conference* (AIAA: American Institute of Aeronautics and Astronautics, 2001), 1–11.

29. R. K. Kapania and S. Raciti, “Nonlinear Vibrations of Unsymmetrically Laminated Beams,” *AIAA Journal* 27, no. 2 (1989): 201–210.

30. S. P. Machado, “Non-Linear Buckling and Postbuckling Behavior of Thin-Walled Beams Considering Shear Deformation,” *International Journal of Non-Linear Mechanics* 43, no. 5 (2008): 345–365.

31. F. Mohri, A. Eddinari, N. Damil, and M. Potier Ferry, “A Beam Finite Element for Non-Linear Analyses of Thin-Walled Elements,” *Thin-Walled Structures* 46, no. 7 (2008): 981–990 A special issue to mark the Retiral of Professor Jim Rhodes, Founding Editor.

32. F. Xie, Y. Qu, W. Zhang, Z. Peng, and G. Meng, “Nonlinear Aerothermoelastic Analysis of Composite Laminated Panels Using a General Higher-Order Shear Deformation Zig-Zag Theory,” *International Journal of Mechanical Sciences* 150 (2019): 226–237.

33. M. Abambres, D. Camotim, and N. Silvestre, “GBT-Based First-Order Analysis of Elastic-Plastic Thin-Walled Steel Members Exhibiting Strain-Hardening,” *IES Journal Part A: Civil and Structural Engineering* 6 (2013): 119–134.

34. J. C. Simo, K. D. Hjelmstad, and R. L. Taylor, “Numerical Formulations of Elasto-Viscoplastic Response of Beams Accounting for the Effect of Shear,” *Computer Methods in Applied Mechanics and Engineering* 42, no. 3 (1984): 301–330.

35. F. Meftah, M. G. Salomon, and J.-M. Reynouard, “Mixed Mode Fracture of a Higher Order Beam Model in Gradient-Dependent Plasticity,” *Revue Européenne des Éléments Finis* 13, no. 8 (2004): 831–839.

36. E. Carrera, “C° Reissner-Mindlin Multilayered Plate Elements Including Zig-Zag and Interlaminar Stress Continuity,” *International Journal for Numerical Methods in Engineering* 39, no. 11 (1996): 1797–1820.

37. E. Carrera, “Transverse Normal Stress Effects in Multilayered Plates,” *Journal of Applied Mechanics, Transactions ASME* 66, no. 4 (1999): 1004–1012.

38. E. Carrera and B. Kroplin, “Zigzag and Iimterlaminar Equilibria Effects in Large-Deflection and Postbuckling Analysis of Multilayered Plates,” *Mechanics of Composite Materials and Structures* 4, no. 1 (1997): 69–94.

39. E. Carrera and G. Giunta, “Refined Beam Theories Based on a Unified Formulation,” *International Journal of Applied Mechanics* 02, no. 1 (2010): 117–143.

40. E. Carrera, G. Giunta, P. Nali, and M. Petrolo, “Refined Beam Elements With Arbitrary Cross-Section Geometries,” *Computers & Structures* 88, no. 5 (2010): 283–293.

41. E. Carrera, G. Giunta, and M. Petrolo, “A Modern and Compact Way to Formulate Classical and Advanced Beam Theories,” in *Developments in Computational Structures Technology* (Saxe-Coburg Publications, 2010), 75–112.

42. E. Carrera and M. Petrolo, “Refined Beam Elements With Only Displacement Variables and Plate/Shell Capabilities,” *Meccanica* 47 (2012): 537–556.

43. V. V. Volovoi, D. H. Hodges, V. L. Berdichevsky, and V. G. Sutyrin, “Asymptotic Theory for Static Behavior of Elastic Anisotropic I-Beams,” *International Journal of Solids and Structures* 36, no. 7 (1999): 1017–1043.

44. V. V. Volovoi and D. H. Hodges, “Theory of Anisotropic Thin-Walled Beams,” *Journal of Applied Mechanics* 67, no. 3 (2000): 453–459.

45. B. Popescu and D. H. Hodges, “On Asymptotically Correct Timoshenko-Like Anisotropic Beam Theory,” *International Journal of Solids and Structures* 37, no. 3 (2000): 535–558.

46. V. L. Berdichevsky, “Equations of the Theory of Anisotropic Inhomogeneous Rods,” in *Doklady Akademii Nauk*, vol. 228 (Russian Academy of Sciences, 1976), 558–561.

47. V. Giavotto, M. Borri, P. Mantegazza, et al., “Anisotropic Beam Theory and Applications,” *Computers & Structures* 16, no. 1 (1983): 403–413.

48. M. Živković, M. Kojić, R. Slavković, and N. Grujović, “A General Beam Finite Element With Deformable Cross-Section,” *Computer Methods in Applied Mechanics and Engineering* 190, no. 20 (2001): 2651–2680.

49. K. Yoon and P.-S. Lee, "Modeling the Warping Displacements for Discontinuously Varying Arbitrary Cross-Section Beams," *Computers & Structures* 131 (2014): 56–69.

50. W. Yu, D. H. Hodges, V. Volovoi, and C. E. S. Cesnik, "On Timoshenko-Like Modeling of Initially Curved and Twisted Composite Beams," *International Journal of Solids and Structures* 39, no. 19 (2002): 5101–5121.

51. W. Yu, V. Volovoi, D. H. Hodges, and X. Hong, "Validation of the Variational Asymptotic Beam Sectional Analysis (VABS)," *AIAA Journal* 40 (2002): 2105–2115.

52. E. Carrera and M. Petrolo, "On the Effectiveness of Higher-Order Terms in Refined Beam Theories," *Journal of Applied Mechanics* 78, no. 2 (2010).

53. M. Petrolo, A. Lamberti, and F. Miglioretti, "Best Theory Diagram for Metallic and Laminated Composite Plates," *Mechanics of Advanced Materials and Structures* 23, no. 9 (2016): 1114–1130.

54. M. Petrolo and E. Carrera, "Best Theory Diagrams for Multilayered Structures via Shell Finite Elements," *Advanced Modeling and Simulation in Engineering Sciences* 6, no. 4 (2019): 1–23.

55. L. Demasi, "∞ 3 Hierarchy Plate Theories for Thick and Thin Composite Plates: The Generalized Unified Formulation," *Composite Structures* 84, no. 3 (2008): 256–270.

56. L. Demasi, "Partially Layer Wise Advanced Zig Zag and HSDT Models Based on the Generalized Unified Formulation," *Engineering Structures* 53 (2013): 63–91.

57. E. Santarpia and L. Demasi, "Large Displacement Models for Composites Based on Murakami's Zig-Zag Function, Green-Lagrange Strain Tensor, and Generalized Unified Formulation," *Thin-Walled Structures* 150 (2020): 106460.

58. M. Petrolo and E. Carrera, "Best Spatial Distributions of Shell Kinematics Over 2D Meshes for Free Vibration Analyses," *Aerotecnica Missili & Spazio* 99 (2020): 217–232.

59. E. Carrera, M. Cinefra, M. Petrolo, and E. Zappino, *Finite Element Analysis of Structures Through Unified Formulation* (John Wiley & Sons, 2014).

60. A. Higdon, E. Ohlsen, W. B. Stiles, J. A. Weese, and W. F. Riley, *Mechanics of Materials* (Prentice Hall, 1985).

Appendix A

Theoretical Bases of the Displacement Models

The complete expansion from Table 1 is given below:

$$
\begin{aligned}
u_x &= u_{x_1} + xu_{x_2} + zu_{x_3} + x^2u_{x_4} + xzu_{x_5} + z^2u_{x_6} + x^3u_{x_7} + x^2zu_{x_8} + xz^2u_{x_9} + z^3u_{x_{10}} \\
&\quad + x^4u_{x_{11}} + x^3zu_{x_{12}} + x^2z^2u_{x_{13}} + xz^3u_{x_{14}} + z^4u_{x_{15}} \\
u_y &= u_{y_1} + xu_{y_2} + zu_{y_3} + x^2u_{y_4} + xzu_{y_5} + z^2u_{y_6} + x^3u_{y_7} + x^2zu_{y_8} + xz^2u_{y_9} + z^3u_{y_{10}} \\
&\quad + x^4u_{y_{11}} + x^3zu_{y_{12}} + x^2z^2u_{y_{13}} + xz^3u_{y_{14}} + z^4u_{y_{15}} \\
u_z &= u_{z_1} + xu_{z_2} + zu_{z_3} + x^2u_{z_4} + xzu_{z_5} + z^2u_{z_6} + x^3u_{z_7} + x^2zu_{z_8} + xz^2u_{z_9} + z^3u_{z_{10}} \\
&\quad + x^4u_{z_{11}} + x^3zu_{z_{12}} + x^2z^2u_{z_{13}} + xz^3u_{z_{14}} + z^4u_{z_{15}}
\end{aligned} \tag{A1}
$$

The reduced expansion from Table 2 is given below:

$$
\begin{aligned}
u_x &= xzu_{x_1} + x^3u_{x_2} + xz^3u_{x_3} \\
u_y &= zu_{y_1} + x^2u_{y_2} + z^3u_{y_3} \\
u_z &= u_{z_1} + z^2u_{z_2} + x^4u_{z_3} + x^2z^2u_{z_4} + z^4u_{z_5}
\end{aligned} \tag{A2}
$$

Appendix B

Explicit Expression of the Nine Fundamental Nuclei

$$
\begin{aligned}
K_{u_xu_xs\tau ji} &= C_{11}\int_L N_jN_i\mathrm{d}y\int_A F_{u_xs,x}F_{u_x\tau,x}\mathrm{d}x\mathrm{d}z + C_{55}\int_L N_jN_i\mathrm{d}y\int_A F_{u_xs,z}F_{u_x\tau,z}\mathrm{d}x\mathrm{d}z \\
&\quad + C_{66}\int_L N_{j,y}N_{i,y}\mathrm{d}y\int_A F_{u_xs}F_{u_x\tau}\mathrm{d}x\mathrm{d}z
\end{aligned} \tag{B1}
$$

$$
K_{u_xu_ys\tau ji} = C_{12}\int_L N_{j,y}N_i\mathrm{d}y\int_A F_{u_xs}F_{u_y\tau,x}\mathrm{d}x\mathrm{d}z + C_{66}\int_L N_jN_{i,y}\mathrm{d}y\int_A F_{u_xs,x}F_{u_y\tau}\mathrm{d}x\mathrm{d}z \tag{B2}
$$

$$K_{u_x u_z s\tau ji} = C_{13} \int_L N_j N_i \mathrm{d}y \int_A F_{u_x s,z} F_{u_z \tau,x} \mathrm{d}x\mathrm{d}z + C_{55} \int_L N_j N_i \mathrm{d}y \int_A F_{u_x s,x} F_{u_z \tau,z} \mathrm{d}x\mathrm{d}z \tag{B3}$$

$$K_{u_y u_x s\tau ji} = C_{12} \int_L N_j N_{i,y} \mathrm{d}y \int_A F_{u_y s,x} F_{u_x \tau} \mathrm{d}x\mathrm{d}z + C_{66} \int_L N_{j,y} N_i \mathrm{d}y \int_A F_{u_y s} F_{u_x \tau,x} \mathrm{d}x\mathrm{d}z \tag{B4}$$

$$\begin{aligned} K_{u_y u_y s\tau ji} = {} & C_{22} \int_L N_{j,y} N_{i,y} \mathrm{d}y \int_A F_{u_y s} F_{u_y \tau} \mathrm{d}x\mathrm{d}z + C_{44} \int_L N_j N_i \mathrm{d}y \int_A F_{u_y s,z} F_{u_y \tau,z} \mathrm{d}x\mathrm{d}z \\ & + C_{66} \int_L N_j N_i \mathrm{d}y \int_A F_{u_y s,x} F_{u_y \tau,x} \mathrm{d}x\mathrm{d}z \end{aligned} \tag{B5}$$

$$K_{u_y u_z s\tau ji} = C_{23} \int_L N_j N_{i,y} \mathrm{d}y \int_A F_{u_y s,z} F_{u_z \tau} \mathrm{d}x\mathrm{d}z + C_{44} \int_L N_{j,y} N_i \mathrm{d}y \int_A F_{u_y s} F_{u_z \tau,z} \mathrm{d}x\mathrm{d}z \tag{B6}$$

$$K_{u_z u_x s\tau ji} = C_{13} \int_L N_j N_i \mathrm{d}y \int_A F_{u_z s,x} F_{u_x \tau,z} \mathrm{d}x\mathrm{d}z + C_{55} \int_L N_j N_i \mathrm{d}y \int_A F_{u_z s,z} F_{u_x \tau,x} \mathrm{d}x\mathrm{d}z \tag{B7}$$

$$K_{u_z u_y s\tau ji} = C_{23} \int_L N_{j,y} N_i \mathrm{d}y \int_A F_{u_z s} F_{u_y \tau,z} \mathrm{d}x\mathrm{d}z + C_{44} \int_L N_j N_{i,y} \mathrm{d}y \int_A F_{u_z s,z} F_{u_y \tau} \mathrm{d}x\mathrm{d}z \tag{B8}$$

$$\begin{aligned} K_{u_z u_z s\tau ji} = {} & C_{33} \int_L N_j N_i \mathrm{d}y \int_A F_{u_z s,z} F_{u_z \tau,z} \mathrm{d}x\mathrm{d}z + C_{44} \int_L N_{j,y} N_{i,y} \mathrm{d}y \int_A F_{u_z s} F_{u_z \tau} \mathrm{d}x\mathrm{d}z \\ & + C_{55} \int_L N_j N_i \mathrm{d}y \int_A F_{u_z s,x} F_{u_z \tau,x} \mathrm{d}x\mathrm{d}z \end{aligned} \tag{B9}$$

Appendix C

Models Used for the Square Cross-Section Beam

This Appendix displays the models utilized for the square cross-section beam, featuring polynomials ranging from first- to fourth-order. The polynomial order denotes the highest order present in any of the displacement variables. For cases where the maximum order is one, Poisson locking corrections is applied.

Table C1 illustrates the models for the bending cases, while Table C2 shows the models for the torsion cases.

TABLE C1 | Models Used for the Bending Case.

First Order (Poisson Locking Correction)
$$\begin{aligned} u_x &= 0 \\ u_y &= z u_{y_1} \\ u_z &= u_{z_1} \end{aligned} \tag{C1}$$
Second Order
$$\begin{aligned} u_x &= xz u_{x_1} \\ u_y &= z u_{y_1} \\ u_z &= u_{z_1} + z^2 u_{z_2} \end{aligned} \tag{C2}$$
Third Order
$$\begin{aligned} u_x &= xz u_{x_1} \\ u_y &= z u_{y_1} + x^2 z u_{y_2} + z^3 u_{y_3} \\ u_z &= u_{z_1} + z^2 u_{z_3} \end{aligned} \tag{C3}$$
Fourth Order
$$\begin{aligned} u_x &= xz u_{x_1} + x^3 z u_{x_2} + x z^3 u_{x_3} \\ u_y &= z u_{y_1} + x^2 z u_{y_2} + z^3 u_{y_3} \\ u_z &= u_{z_1} + z^2 u_{z_2} + x^4 u_{z_3} + x^2 z^2 u_{z_4} + z^4 u_{z_5} \end{aligned} \tag{C4}$$

TABLE C2 | Models Used for the Torsion Case.

First Order (Poisson Locking Correction)
$$\begin{aligned} u_x &= z u_{x_1} \\ u_y &= 0 \\ u_z &= x u_{z_1} \end{aligned} \tag{C5}$$
Second Order
$$\begin{aligned} u_x &= z u_{x_1} + x^2 u_{x_2} + xz u_{x_3} + z^2 u_{x_4} \\ u_y &= x^2 u_{y_1} + xz u_{y_2} + z^2 u_{y_3} \\ u_z &= x u_{z_1} + x^2 u_{z_2} + xz u_{z_3} + z^2 u_{z_4} \end{aligned} \tag{C6}$$
$$\begin{aligned} u_x &= z u_{x_1} \\ u_y &= xz u_{y_1} \\ u_z &= x u_{z_1} \end{aligned} \tag{C7}$$
Third Order
$$\begin{aligned} u_x &= z u_{x_1} + x^3 u_{x_2} + x^2 z u_{x_3} + xz^2 u_{x_4} + z^3 u_{x_5} \\ u_y &= xz u_{y_1} + x^3 u_{y_2} + x^2 z u_{y_3} + xz^2 u_{y_4} + z^3 u_{y_5} \\ u_z &= x u_{z_1} + x^3 u_{z_2} + x^2 z u_{z_3} + xz^2 u_{z_4} + z^3 u_{z_5} \end{aligned} \tag{C8}$$
$$\begin{aligned} u_x &= z u_{x_1} + x^2 z u_{x_2} + z^3 u_{x_3} \\ u_y &= xz u_{y_1} \\ u_z &= x u_{z_1} + x^3 u_{z_2} + xz^2 u_{z_3} \end{aligned} \tag{C9}$$
Fourth Order
$$\begin{aligned} u_x &= z u_{x_1} + x^2 z u_{x_2} + z^3 u_{x_3} + x^4 u_{x_4} + x^3 z u_{x_5} \\ &\quad + x^2 z^2 u_{x_6} + xz^3 u_{x_7} + z^4 u_{x_8} \\ u_y &= xz u_{y_1} + x^4 u_{y_2} + x^3 z u_{y_3} + x^2 z^2 u_{y_4} \\ &\quad + xz^3 u_{y_5} + z^4 u_{y_6} \\ u_z &= x u_{z_1} + x^3 u_{z_2} + xz^2 u_{z_3} \end{aligned} \tag{C10}$$
$$\begin{aligned} u_x &= z u_{x_1} + x^2 z u_{x_2} + z^3 u_{x_3} \\ u_y &= xz u_{y_1} + x^3 z u_{y_2} + xz^3 u_{y_3} \\ u_z &= x u_{z_1} + x^3 u_{z_2} + xz^2 u_{z_3} \end{aligned} \tag{C11}$$